Electroanalytical determination of gallic acid in red and white wine samples using cobalt oxide nanoparticles-modified carbon-paste electrodes.

CHIKERE, C.O., HOBBEN, E., FAISAL, N.H., KONG THOO LIN, P. and FERNANDEZ, C.

2021

Electroanalytical determination of gallic acid in Red and White wine samples using Cobalt Oxide Nanoparticles-modified carbon-paste electrodes

Chrys. O. CHIKERE[a], Emma HOBBEN[a], Nadimul Haque FAISAL[b], Paul KONG-THOO-LIN[a], Carlos FERNANDEZ[a*]

a. *School of Pharmacy and Life Sciences, the Robert Gordon University, Aberdeen, AB10 7GJ, United Kingdom*

b. *School of Engineering, the Robert Gordon University, Aberdeen AB10 7GJ, United Kingdom*

** Corresponding Author. Tel. +44 (0) 1224 262559 E-mail: c.fernandez@rgu.ac.uk*

Highlights

- For the first time synthesised cobalt oxide nanoparticles modified CPE is used for the electrochemical determination of gallic acid
- Differential pulse voltammetry and cyclic voltammetry were used for the characterisation of the modified electrode and also for the determination of gallic acid
- The cobalt oxide nanoparticles modified electrode was used for Red and White wine analysis, producing a third peak current at increased GA concentration in Red wine.

Electroanalytical determination of gallic acid in Red and White wine samples using Cobalt Oxide Nanoparticles-modified carbon-paste electrodes

Chrys. O. CHIKERE[a], Emma HOBBEN[a], Nadimul Haque FAISAL[b], Paul KONG-THOO-LIN[a], Carlos FERNANDEZ[a*]

a. School of Pharmacy and Life Sciences, the Robert Gordon University, Aberdeen, AB10 7GJ, United Kingdom

b. School of Engineering, the Robert Gordon University, Aberdeen AB10 7GJ, United Kingdom

** Corresponding Author. Tel. +44 (0) 1224 262559 E-mail: c.fernandez@rgu.ac.uk*

Abstract

Beverages like wines, have exhibited high level of antioxidant capacity, specifically from compounds like Gallic acid (GA) and their derivatives. GA has shown great importance in the food industry and pharmaceutical industry as a food additive, anti-tumour, anti-viral, and anti-mutagenic agent. Red and white wines from the USA and Australia were electrochemically analysed for GA, using Cobalt oxide nanoparticles modified carbon paste electrode (CoO-NPs-CPE). The electrochemical studies demonstrated an efficient GA (10 mmol L^{-1}) oxidation, with enhanced peak currents from 302 µA to about 405 µA (25 % increase). The limit of detection (LOD) of the modified electrode was 1.52 x 10^{-4} mmol L^{-1} within the concentration range of 1 x 10^{-4} to 1 x 10^{-3} mmol L^{-1}. The CoO-NPs-CPE was successfully used, for the quantitative analysis of GA in red and white wine, showing average recoveries of 97% and 101% respectively. Hence our electrode can be applied for GA quantification in wine matrices.

Keywords: : Cobalt oxide nanoparticles, Carbon paste electrode, Phenolic acids, Gallic acid, Wine samples

1. Introduction

Gallic acid (GA) also known as 3,4,5-trihydrobenzoic acid is a natural phenolic compound, which can be found in plants like tea, grapes, blueberries, walnuts, apples and herbs [1]. GA has been used widely in the food industry as a food additive and as an antiradical, anti-histaminic, anti-mutagenic, anti-tumour and anti-inflammatory chemical compound in the pharmaceutical industry [2–5]. With these properties, GA is seen as an important compound in human diets. This is because it helps in reducing the risk of disease development, by preventing or slowing down molecular oxidation known as oxidative stress in the human body [6]. It should be noted that, oxidative stress has been linked to human diseases such as Alzheimer's disease, Parkinson's disease, cancer, cardiovascular diseases and diabetes [7,8].

With these important uses of GA in the food, drink and pharmaceutical industries, there has been a need for very good analytical methods for its determination in real samples. The analytical methods that have been traditionally used for the determination of GA are high performance liquid chromatography (HPLC) [9], flow injection analysis [10], spectrophotometry [11], and flow injection-chemiluminescence [12]. Although these techniques have shown high sensitivity, they have also needed very expensive equipment, skilled operators, elaborate procedures, and complicated sample preparations. However, electrochemical methods [13,14] have shown advantages that include, high sensitivity, low cost, high selectivity, very short measurement time and are easy to use as compared to the other methods [15–17]. They also provide more information about the reaction mechanism of the compound being analysed [18–21].

Several carbon-based electrochemical sensors have been developed for the determination of GA in food matrices. These include modified glassy carbon electrode (GCE) [22,23], nanomaterials functionalized carbon-based composite electrodes [24], modified-screen-printed electrodes [1] and modified carbon paste electrodes (CPE) [25,26]. Among all

the electrochemical methods and electrode modifications available, carbon paste electrodes modifications appear to be the technique of choice [27,28]. This is due to the low cost of modifying carbon paste electrodes, very low background current, flexibility, ease to effect modification, quick regenerative surface, wide potential window, and its good electrochemical sensing properties, like low ohmic resistance [29–31].

Carbon paste electrodes (CPEs) are a mixture of carbon (graphite) powder and pasting liquid or binder like paraffin oil. Different types of carbonaceous materials and modifiers have been used to develop CPE using different methods. These include carbon nanotubes, graphite, carbon nanofibers, polymers, and nanomaterials [32,33]. These modified carbon paste electrodes have been used as working electrodes in electrochemical experiments aimed at identifying, characterising and quantifying GA. Fayemi & Adekunle, (2015) modified multi-walled carbon nanotubes doped with metal oxide nanoparticles (nickel oxide, zinc oxide and iron oxide nanoparticles), where they were used for the determination of dopamine. On the other hand SiO_2 nanoparticles and TiO_2 nanoparticles [35] respectively, have been used to modify carbon paste electrode, where they were used for the successful determination of GA in, tap water, orange juice and tea samples (black and green teas). However, there are no evidence of metal oxide nanoparticles modified carbon paste electrode that have used for the electrochemical determination of GA in red and white wine samples.

In this era of nanomaterials, different metal oxide nanoparticles have been used to modify CPE for the electrochemical determination of many organic compounds. Most recently ZnO nanoparticles and amorphous zirconium oxide nanoparticles modified CPE have been used for the determination of GA in wine samples [25,36]. With the inherent capacity of transition metals towards electrocatalysis of organic compounds, there was a need to explore other transition metal oxides for the electrochemical determination of GA in food samples. Cobalt oxide (Co_3O_4) nanoparticle is a transition metal oxide nanoparticle that has been used

in electrochemical sensor fabrication. Many different earth-abundant metal oxide nanoparticles like cobalt oxide [26], manganese oxide [37] and nickel oxide [34], have been used as electrode materials for electrochemical determinations. Amongst these compounds, Co_3O_4 nanoparticles have attracted much interest because of their catalytic ability, large surface area, high activity and strong stability [38]. The cobalt oxide nanoparticles have been used in different fields as catalysts, energy storage units and electrochemical sensors [39,40]. Puangjan and Chaiyasith [26] produced a novel Co_3O_4 and ZrO_2 nanoparticles nanocomposite with reduced graphene oxide on to a fluorine-doped electrode for the determination of GA. Their nanocomposite electrode was used for the simultaneous determination of GA, caffeic acid (CA) and protocatechuic acid (PA). Co_3O_4 nanoparticles acted as a composite with zirconia in the determination of GA, CA, and PA. However, the recorded properties of cobalt oxide nanoparticles alone, have not previously been explored for the development of electrochemical sensors for GA determination in wine matrices. Hence, for the first time this study was performed, to use the physicochemical properties of Co_3O_4 nanoparticles to produce a novel nanomaterial-based electrochemical sensor for fast, sensitive, cost-effective, and selective analysis of GA in wine samples.

2. Experimental

2.1 Chemicals and reagents

All chemicals and reagents were of analytical grade and were used as purchased with no further purification unless otherwise stated. Gallic acid (anhydrous), cobalt (II) nitrate hexahydrate ($Co(NO_3)_2.6H_2O$) (purity: ≥ 98%) and sodium hydroxide pellets (NaOH), Graphite powder and paraffin oil were purchased from Sigma Aldrich (London, UK). Potassium ferricyanide (purity: ≥ 99%), potassium chloride (KCl), disodium hydrogen orthophosphate (Na_2HPO_4), sodium dihydrogen orthophosphate (NaH_2PO_4) were from Merck (Darmstadt, Germany). Stock of buffers and gallic acid solutions were kept protected from light at 4 °C. All aqueous

solutions used in this study were made with doubly distilled water with a 18.2 MΩ.cm resistance value. Wine samples were made from commercially available wines from a local store in the city of Aberdeen.

2.2 Instrumentation and Apparatus

Voltammetric measurements and all other electrochemical measurements were carried out using Ivium vertex One potentiostat-galvanostat with Ivium software (Eindhoven, Netherlands). A standard three-electrode cell set-up was used for all the studies, including the modified-CPE as the working electrode, a platinum wire electrode as the auxiliary electrode and an Ag/AgCl (saturated KCl) as a reference electrode. Meanwhile, all potentials recorded in the study were done in reference to the Ag/AgCl reference electrode. The morphology of the electrode surface and elemental analysis were studied using scanning electron microscopy (SEM) and an energy dispersive x-ray analysis (EDXA) spectrum. The measurements were done with a Carl Zeiss variable pressure scanning electron microscope (Oberkochen, Germany), fitted with an Oxford Instrument and energy dispersive X-ray analysis system. The Fourier transform infrared (FTIR) spectrometer used for the chemical bonding analysis was a Thermo Scientific Nicolet iS50 FTIR Spectrometer (Waltham, MA, USA). The thermogravimetric analysis (TGA) measurement was carried out on a PerkinElmer STA 6000 instrument (Waltham, Massachusetts, USA) in an oxygen atmosphere. The size characterisation of the synthesised Co_3O_4 nanoparticles, was done by dynamic light scattering (DLS) using a Malvern Zetasizer Nano ZS (Malvern, UK). All pH measurements were done with a Fisher Scientific Mettler Toledo Benchtop pH meter (Loughborough, UK). Meanwhile, pH adjustments of buffer solutions were done with sodium hydroxide (1×10^2 mmol L^{-1}) for pH increase or phosphoric acid (10 mmol L^{-1}) to lower the pH. HPLC analysis was carried out with a Shimadzu HPLC system consisting of LC-20AD prominence liquid chromatography,

using a SIL-20A autosampler and an SPD-M20A diode array detector (Kyoto, Japan). The columns used for the measurements were the C_{18} ODS Hypersil-Keystone LC -18 (150 x 4.6 mm i.d., 3mm) in conjunction with a Supelguard LC 18 (2cm x 2.1 mm i.d.) guard cartridge column. The software used for all the analysis was the Shimadzu LC solution software (Kyoto, Japan).

2.3 Synthesis of Cobalt Oxide nanoparticles

Cobalt oxide nanoparticles (Co_3O_4) was synthesised by a co-precipitation method previously described [41]. Cobalt (II) nitrate hexahydrate ($Co(NO_3)_2.6H_2O$) (5.82 g in 20 ml; 1M) and NaOH in a 1:2 M ratio (molar ratio), were dissolved in distilled water (20 mL), while stirring constantly. Using the molar ratio, NaOH solution (2×10^3 mmol L^{-1}) was added dropwise to $Co(NO_3)_2.6H_2O$ (1×10^3 mmol L^{-1}), under constant stirring for 2 hr at room temperature (~ 25 °C). The solution mixture was then left to settle overnight at room temperature. Cobalt hydroxide sludge was found to settle at the bottom of the flask the next day. Meanwhile, the excess solution on top of the sludge was carefully decanted and the precipitated sludge was then separated using a centrifuge (15000 RPM for 15 mins). The residue was then heated for 5 hrs at 80 °C to form a black colour compound (~ 80 % yield).

The cobalt oxide nanoparticles synthesised were characterised by measuring the particle sizes with a Zetasizer and other physical structures studied, using SEM, EDXA, and FTIR.

2.4 Preparation of the modified Carbon Paste Electrodes

Graphite powder and paraffin oil binder mixture ratio for the bare CPE were optimised for the best results. The bare CPE was prepared by thoroughly mixing and grinding in graphite powder and paraffin oil (70:30; w/w) ratio into a homogenous paste using an agate mortar and pestle for 30 min. The homogenous paste was then transferred into a solvent-resistant Teflon tube of

2.87 mm internal radius and smoothened on a weighing paper. The other end of the filled Teflon tube was connected to copper wire to provide a connection. The modified CPE was prepared by mixing graphite powder, Co_3O_4 nanoparticles and paraffin oil in a 60:10:30 (w/w/w) ratio. The mixture was thoroughly grounded with an agar mortar and pestle for about 30 mins and then the paste was transferred into a Teflon tube.

2.5 Preparation of wine samples

The measurement of the GA content in the wine samples was carried out using differential pulse voltammetry (DPV), by recording the voltammograms produced by spiked samples of the wine. Each wine sample (1 mL) was made up to 10 mL in a voltammetric cell with phosphate buffer solution (10 mmol L^{-1}, pH 2.0). In all the samples, their pH was adjusted to 2.0 with phosphoric acid (10 mmol L^{-1}). In measuring the spiked samples of the wine, aliquots amount of gallic acid solution ((1 mL, 10 mmol L^{-1}) were added to the wine sample, while stirring for 2 mins followed by the recording of the voltammogram.

2.6 Electrochemical measurements

The electrochemical oxidation of gallic acid on the surface of the cobalt oxide nanoparticles-modified carbon paste electrode (CoO-NPs-CPE) was carried out using CV and DPV. The cyclic voltammograms were carried out in a potential scan range of 0.0 to +1.5 V and a scan rate of 100 mVs^{-1}. For the differential pulse voltammetry, measurements were done at a potential scan range of 0.0 to +1.5 V, with a pulse amplitude of 0.08 V and a pulse period of 0.2 s. All the electrochemical analysis of GA on the surface of all the carbon paste electrodes, were done in phosphate buffer (1×10^2 mmol L^{-1}, pH 2.0) at room temperature.

Electrochemical impedance spectroscopy (EIS) of the bare and modified CPE was carried out to ascertain the impedance changes between the bare and modified electrodes. The frequency

range of 100 KHz-0.1 Hz was used for the EIS measurement at a potential of 0.4 V in 1 x 10^2 mmol L^{-1} KCl containing 5 mmol L^{-1} $[Fe(CN)_6]^{3-/4-}$ redox solution.

3. Results and discussion

3.1 Characterisation of Co_3O_4 nanoparticles-modified CPE

The synthesised Co_3O_4 nanoparticles were analysed with SEM, EDX, FTIR, and TGA. The SEM and EDXA were used to study the morphology and elemental composition of the nanoparticles. Fig 1 shows the SEM images and EDXA analysis, with the morphology, microstructure, and the elemental composition of the Co_3O_4 nanoparticles (Fig 1(a)) and the CoO-NP-CPE (Fig 1(b)). The SEM images show non-homogenous size distributions of cobalt oxide nanoparticles, ranging from 60 nm to 280 nm as demonstrated by the Dynamic Light Scattering (DLS) results (Fig. 1(d)). This is in line with Yang, Liu, Martens, & Frost, (2010) who showed particles sizes of 100 nm to 600 nm. The elemental composition (Fig 1(c)) of the nanosized cobalt oxide compound shows the proportional atomic ratio (3:4) of cobalt and oxygen. Meanwhile, the CoO-NP-CPE paste (Fig 1(b)), shows also a non-homogeneous morphology, with the milky coloured presence of the paraffin oil binder. The nanosized composition of the CoO-NP-CPE as shown in Fig 1(b) contributed to the peak current enhancement and provided better mass transport when used, as seen in later experiments.

Fig 1. (a) The SEM Image of Cobalt oxide nanoparticles showing the morphology of the nanoparticles with (Inset) Co_3O_4 in 100 nm (**b)** SEM Image of CoO-nano-CPE, with the paraffin holding the Cobalt oxide nanoparticles and graphite together **(c)** EDXA analysis of Cobalt oxide nanoparticles **(d)** Size distribution of cobalt oxide nanoparticles using a Zetasizer.

The FTIR characterisation of the cobalt oxide nanoparticles was carried out in the mid-infrared range (MIR) of 400 to 4000 cm^{-1} (Fig. S1), set in transmittance mode, with a resolution of 4 cm^{-1} and scanned 32 times. From the FTIR spectrum, the absorption peak at 558 cm^{-1} is assigned to the Co-O stretching vibration, as octahedrally coordinated by the Co^{3+} ions.

Meanwhile, the 658 cm^{-1} absorption band is attributed to the bridging vibration in Co^{2+} ion, which in this case is tetrahedrally coordinated [43]. The strong absorbance as seen at 1340 cm^{-1} could be attributed to traces of unreacted Na-OH. On the other hand, water absorbed by the Co_3O_4 nanoparticles is linked to the 3400 – 3600 cm^{-1} bands attributed to the O-H stretching and bending [44].

The thermogravimetric analysis (TGA) of the cobalt oxide nanoparticles (Fig. S2) was carried to ascertain the thermal stability of the nanoparticles. The oxygen flow rate of the TGA was 20 mL min^{-1} and the rate of heating of the sample was 10 °C min^{-1} using α-alumina crucibles, from room temperature to 900 °C. From the analysis, the TGA profile showed three main step-downs. The first step started with an initial weight loss up to 150 °C which could be mainly attributed to the evaporation of water molecules absorbed on the CoO-NP. The temperature then rises for the second step of weight loss from 210 °C to 500 °C which is attributed to the volatilisation and combustion of organic species with the formation of the pyrochlore phases [45]. The last weight loss step from 500 °C to 650 °C is attributed to the decomposition of the pyrochlore phases to the CoO-NPs pure phases. With no further significant weight loss up to 900 °C on the TGA curve, suggesting the formation of a decomposed cobalt oxide product.

The results of the characterisation confirm the synthesis of cobalt oxide nanoparticles which were used for the modification of the carbon paste electrode.

3.2 Electrochemical characterisation of CoO-NPs-CPE

The electrochemical determination of GA (10 mmol L^{-1}, pH 2.0) in phosphate buffer (1×10^2 mmol L^{-1}) was carried out using bare CPE and the cobalt oxide nanoparticles-modified CPE (CoO-NPs-CPE). Using Cyclic voltammetry as shown in Fig 2(a), at a scan rate of 100 mVs^{-1} and a scan potential range of 0 to +1.5 V in the absence of GA; there was no anodic peak current. However, when GA (10 mmol L^{-1}, pH 2.0) was measured using CPE and the CoO-

NPs-CPE, there were noticeable anodic peak currents respectively at a peak potential of 0.61 V (Fig. 2(a)). The peak currents produced by CoO-NPs-CPE showed up to a 25% positive enhancement of the peak current produced by the CPE. This demonstrates the effect of the Co_3O_4 nanoparticles on the CPE electrode, as it increases the electroactive surface area of the electrode. The effect of the CoO-NPs on the CPE was also demonstrated in the measurement of 5 mmol L^{-1} $[Fe(CN)_6]^{3-/4-}$ redox solution (Fig.2(b)), where the modified electrode (CoO-NPs-CPE) shows an enhanced peak current relative to the peak current of the bare CPE.

Electrochemical impedance spectroscopy (EIS) serves as an effective method to monitor and understand the chemical changes that have occurred in the course of modifying the electrodes from CPE to CoO-NPs-CPE. The EIS measurement was carried out in a $[Fe(CN)_6]^{3-/4-}$ (5 mmol L^{-1}) redox solution and the Nyquist plot produced (Fig 2(c)). The Nyquist plot of the impedance spectra shows a semi-circular domain and smaller linearly inclined domain. The semi-circular portion at the high frequencies indicates the reaction had undergone an electron transfer limited process. Meanwhile, the diameter of the semi-circular portion provides us with the electron-transfer resistance (R_{ct}). The Nyquist plot of the impedance of the bare CPE (black curve) (Fig 2(c)) exhibits an apparent interfacial electron-resistance (R_{ct}). For the CoO-NPs-CPE the semi-circular part shows a reduced diameter as compared to the bare CPE, depicting an increased and facilitated interfacial electron transfer. This shows that, the use of cobalt oxide nanoparticles to modify the CPE helps to decrease the electron transfer resistance, as compared to the bare CPE.

Fig 2. (a) Cyclic voltammetry of GA (10 mmol L^{-1}) at the CoO-NPs-CPE and bare CPE in 1 x 10^2 mmol L^{-1} phosphate buffer of pH 2.0 at a scan rate of 100 mVs^{-1}. **(b)** The cyclic voltammograms of 5 mmol L^{-1} $[Fe(CN)_6]^{3-/4-}$ redox solution, using bare CPE and CoO-NPs-CPE, **(c)** Nyquist plot showing the EIS measurements of $[Fe(CN)_6]^{3-/4-}$ (5 mmol L^{-1}) using the bare CPE and CoO-NPs-CPE (inset) The equivalent circuit used for the calculation

The effective reactive surface area of the modified electrode was also studied, using the electrodes to determine KCl (1 x 10^2 mmol L^{-1}) solution in $[Fe(CN)_6]^{3-/4-}$ (1 mmol L^{-1}) using CV at different scan rates (100, 200, 250, 300, 350, 400, 450 mVs^{-1}). From the voltammograms produced (Fig. S3(a)) the plots of peak currents (I_p) vs square root of scan rate ($v^{1/2}$) (Fig. S3(b)) was generated and used for the determination of reactive surface area, using the Randles-Śev□ik equation thus: -

$$I_{pa} = (2.69\ x\ 10^5) n^{2/3} A\, D^{1/2} v^{1/2} C_0 \ldots\ldots\ldots \text{Eq. 1}$$

Where I_{pa} is the anodic peak current, n is the number electrons involved in the transfer, in the course of the redox reaction, A is the effective surface area of the electrode, D is the diffusion coefficient for $K_3[Fe(CN)_6]$ which is 7.6 x 10^{-6} cm^2s^{-1}, v is the scan rate and C is the concentration of $K_3[Fe(CN)_6]$. From the plot of I_p vs $v^{1/2}$ the anodic peak currents produced the linear regression equation of I_p = 64.827 $v^{1/2}$ + 176.92, R^2 = 0.9983 and the cathodic peak currents gave I_p = -97.399 $v^{1/2}$ - 492.72, R^2 = 0.9997. Using the Randles-Śev□ik equation, the effective surface area was calculated to be 0.088 cm^2 for CPE and 0.321 cm^2 for the CoO-NPs-CPE. From the calculation, it can be seen that the effective surface area of the CPE was less than that of the CoO-NPs-CPE. This shows that, the cobalt oxide nanoparticles served as an effective modifier that increased the surface area of the electrode.

3.3 Electrochemical behaviour of gallic acid on the CPE

The electrochemical behaviour of the GA on the surface of the modified and unmodified electrodes was studied using CV. GA (10 mmol L^{-1}, pH 2.0) was oxidised on the faces of three different electrodes, in a phosphate buffer (10 mmol L^{-1}), at a scan rate of 100 mVs^1. As shown in Fig. 3, bare CPE, bulk Co_3O_4 (bulk-CoO-CPE) and CoO-NPs-CPE produced anodic peak currents in the scan potential range of 0 to +1.5 V at room temperature. Meanwhile, there was no peak seen when the electrodes were used on phosphate buffer alone,

through the same potential range of 0.0 to +1.5 V. The voltammograms (Fig.3) shows the anodic peak currents produced by all the electrodes in the presence of GA, as two oxidation peaks. The first oxidation peak is much more prominent than the second and is the peak used for the determination of GA.

The oxidation peak current of GA when using bare CPE, bulk-CoO-CPE and CoO-NPs-CPE produced peak current at peak potentials of 0.6 - 0.67 V as can be seen in Fig 3. From these voltammetric results, CoO-NPs-CPE showed the highest oxidation peak current as compared to the other electrodes. This demonstrates the effect of the cobalt oxide nanoparticles in the CPE modification and the GA oxidation, where the peak current was enhanced.

Fig 3. Cyclic voltammograms of 10 mmol L^{-1} GA at Co_3O_4 nanoparticles-modified CPE, bulk Co_3O_4 nanoparticles-modified CPE and bare CPE in 1 x 10^2 mmol L^{-1} phosphate buffer of pH 2.0 at a scan rate of 100 mVs^{-1}

On the other hand, the bulk CoO-CPE that was used for the modification of CPE, produced a negative effect on GA oxidation. The peak current produced by the bulk CoO-CPE was less than those of the bare CPE and CoO-NPs-CPE. Showing peak currents of the electrodes as CoO-NPs-CPE > bare CPE > bulk CoO-CPE. This might be as a result of reduced electroactive surface area attributed to the bulk cobalt oxide, as compared to the cobalt oxide nanoparticles in the carbon paste electrode. This is because the increased electroactive surface area of metal oxide nanoparticles tend to enhance the peak currents of the modified electrode [22,36,46].

The enhanced peak current of the oxidised GA, when CoO-NPs-CPE was used may be due to the higher surface area and the adsorptive capacity of the modified electrode surface. The more GA is adsorbed on the surface of the modified electrode the higher is the accumulation efficiency and increase in the surface concentration. However, it can be observed from the voltammograms shown in Fig 3 that, the peak potential at the determination of GA on CoO-NPs-CPE shows a little positive shift of 0.01 V as compared to that of the bare CPE. This

shows that, the cobalt oxide nanoparticles did not catalyse the oxidation of GA, but enhanced the peak current generated by the oxidation reaction. Had there been any catalysis, the peak potential would have had a negative shift to the bare CPE. The reduction of peak potential would have meant a faster reaction with less overpotential. Hence, the peak current enhancement was not attributed to electrocatalysis but the increased electroactive surface area from the cobalt oxide nanoparticles used

Furthermore, the two oxidation peaks produced by GA on the surfaces of the electrodes in the course of the anodic sweep from 0.0 to 1.6 V is consistent with other GA measurements in literature [22,36,47,48]. The first peak is attributed to the formation of the semiquinone radical, which is then oxidised to the quinone form as the second peak with poor resolution. The first peak is from the galloyl group and the second peak then develops from the third hydroxyl (-OH) group on the galloyl moiety of the gallic acid. This is because, normally the carboxylic group (-COOH) is oxidised at a peak potential of 2.0 V and give off CO_2 as bi-product [49]. Meanwhile, the two oxidation peaks, in this case, occur at 0.61 V and 0.9 V. One electron and one proton are said to have been transferred in each of the reaction processes, without any peak on the reverse scan. This confirms an irreversible reaction. The gallic acid oxidation mechanism (Fig. S4) depicts the oxidation of GA in acidic condition, showing the two peaks.

3.4 Effect of pH on Gallic Acid Oxidation

The effect of the pH on the electroanalytical performance of the CoO-NPs-CPE on the detection of GA, was studied using CV and the voltammograms recorded as seen in Fig. S5(a) and S5(b). The modified electrode was used to measure GA (1 mmol L^{-1}) in phosphate buffer (1 x 10^2 mmol L^{-1}) at pH values of 2.0, 4.0, 6.0, 8.0 and 10, at a scan rate of 100 mVs^{-1}. From the literature [22] it can be seen that GA oxidation is influenced by a protonation reaction (Fig.

S5), thus suggesting its oxidation is influenced by the pH condition of the buffer. From the voltammograms recorded in Fig. S5(a) and S5(b), the anodic peak currents of GA decreased with the increasing pH values and a negative shift of the anodic peak potentials. The best-resolved peak current from the voltammograms, was the peak current produced at pH 2.0. It could be deduced from the results that the oxidation procedure of gallic acid is related to H^+ ions of the solution, as seen in Fig. S4. The results show that the GA oxidation peak currents decrease linearly with the increase in pH value of the solution. This produce a non-linear equation of I_p = -2107 pH + 32.755 and R^2 = 0.9203 (Fig. S5(d)). Meanwhile, the plot of peak potential (E_p) vs pH showed a good linear relationship in the pH range of 2.0 to 8.0, that produced a linear regression equation of E_p = -0.058 pH + 0.655 and R^2 = 0.9938. From the linear regression equation, the slope E_p/pH of the regression line is 58 mV/pH. This is almost equivalent to the Nernstian value of 59 mV/pH at room temperature, for an equal number of protons and electrons transfer reactions. The oxidation reaction of GA on the surface of CoO-NPs-CPE is two electrons and two protons process (Fig. S4). With the positive shift of the oxidation peak potential as the pH decreases, it indicates that, GA needs higher potential for its oxidation at low pH values. However, based on the peak currents produced, pH 2.0 was used for subsequent experiments, which is in line with other works in the literature [22,36,47].

Just looking at the colour changes observed (Fig. S6) with GA in different pH, suggests an influence of pH in GA oxidation. UV spectrophotometer was used to measure the colour changes of the different GA acid solutions at different pHs at 280 nm and the absorbance recorded (Table 1). From the absorbance results, the higher pH solutions show an extensive change in colour which can be attributed to the reduction of GA caused by its exposure to light. This phenomenon just confirms the effect of pH in GA oxidation. Hence all GA solutions were protected from light by wrapping the glassware with aluminium foil and refrigerated at 4 °C.

Table 1. The absorbance values of GA (1 mmol L^{-1}) at different pH at the wavelength of 280nm

3.5 Effect of scan rate on Gallic Acid Oxidation

The influence of the scan rate on the electrooxidation of GA on the surface of the CoO-NPs-CPE was also studied using CV. GA (1 mmol L^{-1}) in phosphate buffer (1 x 10^2 mmol L^{-1}, pH 2.0) was measured, within the scan rate range of 25 – 1000 mVs^{-1}, at room temperature (Fig. S7(a)). From the results of the scan rate, it can be seen that the oxidation peak currents (I_p) of GA increased linearly with the scan rate (v) within the range of 50 – 400 mVs^{-1}. This is an indication that, the electrode interaction process was an adsorption-controlled process, with a linear regression equation of $I_p = 0.1979\ v + 11.831$ with $R^2 = 0.9966$ (Fig. S7(b)) [50].

On the other hand, the peak potentials show a slight positive shift as the scan rate increases, with a linear increase in peak currents. This suggests that there is a kinetic limitation in GA reaction at the surface of CoO-NPs-CPE.

3.6 Effect of CoO-NPs concentration on the CPE mixture

The effect of the concentration of cobalt oxide nanoparticles (CoO-NPs) in preparing the modified-carbon paste electrode was studied using CV. Cobalt oxide nanoparticles (0.5 g, 0.1 g, 0.15 g and 0.2 g) were weighed and mixed with graphite powder of appropriate ratio (Making up the graphite to 70% of the CPE and Paraffin 30%; w/w). The modified electrodes were then used for the electrochemical determination of GA (10 mmol L^1) in phosphate buffer solution (1 x 10^2 mmol L^{-1}, pH 2.0) and a scan rate of 100 mVs^{-1}. From the results (Fig. S8), the CoO-NPs-CPE that had 10% cobalt oxide nanoparticles showed the highest current and most resolved peak. Therefore, the 10% cobalt oxide nanoparticles-modified CPE was subsequently used for further experiments and electrochemical determinations of GA.

3.7 Calibration curve and the limit of detection of GA determination

Differential pulse voltammetry (DPV) was used for the determination of the calibration curve and the limit of electrochemical detection (oxidation) of GA at the surface of the CoO-NPs-CPE. The DPV was recorded at a potential range of 0 to + 1.5 V, the scan rate of 100 mVs^{-1}, pulse amplitude of 80 mV and a pulse period of 0.2 s. Using the optimised conditions voltammograms were recorded from the oxidation of increasing concentrations of GA in phosphate buffer (1 x 10^2 mmol L^{-1}, pH 2.0) on the surface of the CoO-NPs-CPE (Fig. 4). The recorded results were then used for the determination of the calibration curve and the limit of detection (LOD) of the modified electrode.

From the results in Fig. 4, it is observed that the anodic peak currents changed linearly with the increasing GA concentration from the concentration range of 1 x 10^{-4} to 1 x 10^{-2} mmol L^{-1}. However, the linearity of the increasing peak current relative to the increase GA concentration was specifically between 1 x 10^{-4} to 1 x 10^{-3} mmol L^{-1}, within the examined concentration range of 1 x 10^{-4} to 1 x 10^{-2} . DPV produced voltammograms of GA with two peaks at peak potentials of 0.55 V and 0.9 V, respectively. The peak potential showed a slight positive shift with increasing concentration of gallic acid, as can be seen in Fig 4 (a). The corresponding analytical calibration curve, as shown in Fig 4 (a) inset shows a linear relationship between the peak current (I_p) and the gallic acid concentration as seen in Fig 4 (a)

Fig 4. (a) Differential voltammograms of various concentrations of GA at CoO-nano-CPE in a 1 x 10^{-2}mmol L^{-1} phosphate buffer at pH 2.0 at scan rate of 100 mVs^{-1}, with voltammograms (a-j) that corresponds to the following concentrations a) Blank PBS, b) 1 x 10^{-4} mmol L^{-1}, c) 2.5 x 10^{-4} mmol L^{-1}, d) 5 x 10^{-4} mmol L^{-1}, e) 7.5 x 10^{-4} mmol L^{-1}, f) 1 x 10^{-3} mmol L^{-1}, g) 2.5 x 10^{-3} mmol L^{-1}, h) 5 x 10^{-3} mmol L^{-1}, i) 7.5 x 10^{-3} mmol L^{-1}, j) 1 x 10^{-2} mmol L^{-1} (inset) Plot of concentration of GA against peak currents. **(b)** The plot of the Peak Current (I_p) against the concentration of GA, showing the effect of concentration on the electrochemical behaviour of increasing GA concentration, using CoO-nano-CPE at a scan rate of 100 mVs^{-1}

The first and major peaks from the DPV voltammograms produced from the different GA concentrations were used to create the calibration graph (Fig. 4(a) inset and Fig. 4(b)). The

linear relationship is depicted in the linear regression equation, which is also the calibration curve as I_p = 11285.86 C – 0.07936 (I_P: μA, C: mmol L^{-1}) and R^2= 0.9934 from 1 x 10^{-4} mmol L^{-1} to 1 x 10^{-2} mmol L^{-1} as seen Fig. 4 (b). Meanwhile, the limit of detection (LOD) defined as (3 x Std_{Blank})/m where Std_{Blank} is the standard deviation of the blank and m is the slope; was found to be 1.52 x 10^{-4}mmol L^{-1} (S/N=3) and concentration range 1 x 10^{-4} mmol L^{-1} to 1 x 10^{-2} mmol L^{-1}. The CoO-NPs-CPE showed a relatively wide linear dynamic range and the low limit of detection was comparable to others in the literature, where the limit of detections are between the range of 2.09 x 10^{-6} to 1.5 x 10^{-9} mmol L^{-1} [22,25,26,48]. This is based on the fact that, the maximum permitted GA concentration in the EU and North America antioxidant limit guidelines is 1.2 x 10^2 mmol L^{-1} to 6.0 x 10^3 mmol L^{-1}. The LOD from this electrode is below this limit, hence would be suitable for use in GA determination of GA concentration even at high concentrations.

Table 2. Metal Oxide Nanoparticles (MO-NPs) and Metal Nanoparticles composites in different electrochemical sensor systems for the determination of Gallic acid.

3.8 Reproducibility and repeatability of the method

The reproducibility of using CoO-NPs-CPE for the electrochemical determination of GA (5 x 10^{-1} mmol L^{-1}) was studied using DPV. This was carried out by measuring the GA with six newly prepared CoO-NPs-CPE (prepared on different days). The results (Fig. S9(a)) show a relative standard deviation of the peak currents produced was 4.56%. This suggests a relatively good reproducibility of the preparation procedure of the electrodes.

Furthermore, the repeatability of the method was studied, by taking six independent measurements of GA (5 x 10^{-1} mmol L^{-1}) in phosphate buffer (1 x 10^2 mmol L^{-1}, pH 2.0) with a CoO-NPs-CPE. From the result of the measurement (Fig. S9(b)), the relative standard deviation of the voltammograms produced was 0.66%, showing a very good repeatability.

3.9 Stability of the modified electrode

The long-term storage stability of the modified electrode (CoO-NPs-CPE) was studied by keeping the electrode at room temperature, then used twice to detect GA (5 x 10^{-1} mmol L^{-1}) after 15 and 30 days, respectively using DPV. The recorded voltammograms for the first day, 15th day and 30th day showed peak currents with RSD of 6.32% (Fig. S10), which demonstrated a good stability.

3.10 Interference study

The selectivity of the CoO-NPs-CPE was studied by determination of GA (10 mmol L^{-1}), using DPV conducting interference experiments in the presence of different metals ions (K^+, Cl^-, Na^+, Fe^{3+}) and other organic (antioxidant) compounds (ascorbic acid and quercetin). The use of those cations and organic compounds was because of their potential properties to complex or interfere with the electrochemical determination gallic acid respectively [51]. The results in Fig. S11, showed RSD values of less than 5%, suggesting the ions and the organic compound did not interfere with the determination of GA.

3.11 Analytical application of the modified electrode in the determination of GA in Wine

The modified carbon paste electrode was used for the determination of GA content in red and white wine. The presence of GA in red and white wine samples have previously been analysed by electrochemical determination and HPLC analysis [22,50]. The wine (Australia and USA) samples were diluted with phosphate buffer (10 mmol L^{-1}) and the pH adjusted to 2.0 with phosphoric acid (1 x 10^2 mmol L^{-1}). The wine samples were then spiked with standard solutions of GA to obtain a GA range from 0 – 2.3 mmol L^{-1} followed by the recording of their corresponding DPV voltammograms Table 3, (Fig. S12(a) and Fig. S12(b)). The results

showed that with CoO-NPs-CPE exhibited anodic peaks in the absence of GA. This suggests that the cobalt oxide modified CPE electrode detected GA or showed an antioxidant capacity in these wine samples (Fig. S12). The anodic peak current produced by the wine sample is generally attributed to the total antioxidant capacity of the sample as described by Kilmartin et al., (2001), Makhotkina and Kilmartin, (2009) and Lopez-Velez et al., (2003) [52–54]. Hence, the use of the standard addition of GA to confirm the presence of GA in the wine sample. On the other hand the confirmation of the presence of GA in the wine samples was carried out using HPLC (Fig S14) and the results were in line with Ragusa et al., (2019); where they found GA in Negroamaro and Primitivo red wines from Salento.

Table 3. Results of the analysis of GA in spiked Red Wine and White Wine

Furthermore, in the course of the determination of GA in the red wine sample there was an unusual observation. As the standard solution of GA, that was being used for the spiking was increased, there was a third peak observed in the voltammograms (Fig. S13). In the determination of GA in the red wine using CoO-NPs-CPE, the normal first and second peaks of GA were noticed at peak potentials of 0.59 V and 1.02 V, while, the third unusual peak is seen at a peak potential of 0.76 V. This third peak could be attributed to the activation of another compound in the red wine as the GA concentration increases in the red wine sample.

4. Conclusions

In this work a novel Co_3O_4 nanoparticles-modified carbon paste electrode was successfully prepared and used for the electrochemical determination of GA in phosphate buffer (1×10^2 mmol L^{-1}, pH 2.0) using CV and DPV. The CoO-NPs-CPE showed excellent activity on GA oxidation and an enhancement in peak current of 25% as compared to the bare CPE. The modified carbon paste electrode demonstrated good stability, reproducibility, and repeatability. The selectivity of the modified electrode was demonstrated by using the electrode to determine

GA in the presence of some interferant foreign species, like K^+, Cl^-, Na^+, Fe^{3+}, ascorbic acid and quercetin. The characteristics of the modified electrode led to its use in the determination of GA in red and white wine. With the low cost and ease of fabrication, the CoO-NPs-CPE would be a suitable sensor for the determination of other phenolic compounds in food matrices.

Acknowledgement

The authors would want to acknowledge the work done by the research and teaching laboratory staff of the School of Pharmacy and Life Sciences of the Robert Gordon University.

Conflict of interest

Dr. Chrys. O. Chikere declares that he has no conflict of interest. Ms. Emma Hobben declares that she has no conflict of interest. Dr. Nadimul H Faisal declares that he has no conflict of interest. Professor Paul Kong-Thoo-Lin declares that he has no conflict of interest. Dr. Carlos Fernandez declares that he has no conflict of interest.

Appendix A. Supplementary data

Reference

[1] N. Raja, T. Kokulnathan, S.M. Chen, W.C. Liao, T. Sakthi Priya, Amperometric detection of gallic acid based on electrochemically activated screen printed carbon electrode, Int. J. Electrochem. Sci. 12 (2017) 4620–4629. https://doi.org/10.20964/2017.06.22.

[2] Y.C. Chia, R. Rajbanshi, C. Calhoun, R.H. Chiu, Anti-Neoplastic effects of gallic acid, a major component of toona sinensis leaf extract, on oral squamous carcinoma cells, Molecules. 15 (2010) 8377–8389. https://doi.org/10.3390/molecules15118377.

[3] C. Dalla Pellegrina, G. Padovani, F. Mainente, G. Zoccatelli, G. Bissoli, S. Mosconi,

G. Veneri, A. Peruffo, G. Andrighetto, C. Rizzi, R. Chignola, Anti-tumour potential of a gallic acid-containing phenolic fraction from Oenothera biennis, Cancer Lett. 226 (2005) 17–25. https://doi.org/10.1016/j.canlet.2004.11.033.

[4] B. Bajpai, S. Patil, A new approach to microbial production of gallic acid., Braz. J. Microbiol. 39 (2008) 708–11. https://doi.org/10.1590/S1517-838220080004000021.

[5] J. Jayamani, G. Shanmugam, Gallic acid, one of the components in many plant tissues, is a potential inhibitor for insulin amyloid fibril formation, Eur. J. Med. Chem. 85 (2014) 352–358. https://doi.org/10.1016/j.ejmech.2014.07.111.

[6] I. Pinchuk, H. Shoval, Y. Dotan, D. Lichtenberg, Evaluation of antioxidants: Scope, limitations and relevance of assays, Chem. Phys. Lipids. 165 (2012) 638–647. https://doi.org/10.1016/j.chemphyslip.2012.05.003.

[7] R. Nowak, M. Olech, N. Nowacka, Plant Polyphenols as Chemopreventive Agents, Polyphenols Hum. Heal. Dis. 2 (2013) 1289–1307. https://doi.org/10.1016/B978-0-12-398456-2.00086-4.

[8] A.A. Zanwar, S.L. Badole, P.S. Shende, M. V. Hegde, S.L. Bodhankar, Role of Gallic Acid in Cardiovascular Disorders, Elsevier Inc., 2013. https://doi.org/10.1016/B978-0-12-398456-2.00080-3.

[9] M. Tasioula-Margari, E. Tsabolatidou, Extraction, Separation, and Identification of Phenolic Compounds in Virgin Olive Oil by HPLC-DAD and HPLC-MS, Antioxidants. 4 (2015) 548–562. https://doi.org/10.3390/antiox4030548.

[10] W. Phakthong, B. Liawruangrath, S. Liawruangrath, Determination of gallic acid with rhodanine by reverse flow injection analysis using simplex optimization, Talanta. 130 (2014) 577–584. https://doi.org/10.1016/j.talanta.2014.06.024.

[11] Z. Chen, R. Bertin, G. Froldi, EC50 estimation of antioxidant activity in DPPH* assay using several statistical programs, Food Chem. 138 (2013) 414–420. https://doi.org/10.1016/j.foodchem.2012.11.001.

[12] S. Parveen, M.S. Aslam, L. Hu, G. Xu, Electrogenerated chemiluminescence protocols and applications, Springer Berlin Heidelberg, 2013.

[13] V. Andrei, E. Sharpe, A. Vasilescu, S. Andreescu, A single use electrochemical sensor based on biomimetic nanoceria for the detection of wine antioxidants, Talanta. 156–157 (2016) 112–118. https://doi.org/10.1016/j.talanta.2016.04.067.

[14] Madhusudhana, G. Manasa, A.K. Bhakta, Z. Mekhalif, R.J. Mascarenhas, Bismuth-nanoparticles decorated multi-wall-carbon-nanotubes cast-coated on carbon paste electrode; an electrochemical sensor for sensitive determination of Gallic Acid at neutral pH, Mater. Sci. Energy Technol. 3 (2020) 174–182. https://doi.org/10.1016/j.mset.2019.10.001.

[15] H. Karimi-Maleh, F. Karimi, Y. Orooji, G. Mansouri, A. Razmjou, A. Aygun, F. Sen, A new nickel-based co-crystal complex electrocatalyst amplified by NiO dope Pt nanostructure hybrid; a highly sensitive approach for determination of cysteamine in the presence of serotonin, Sci. Rep. 10 (2020) 1–13. https://doi.org/10.1038/s41598-020-68663-2.

[16] H. Karimi-Maleh, F. Karimi, M. Alizadeh, A.L. Sanati, Electrochemical Sensors, a Bright Future in the Fabrication of Portable Kits in Analytical Systems, Chem. Rec. (2020). https://doi.org/10.1002/tcr.201900092.

[17] Z. Shamsadin-Azad, M.A. Taher, S. Cheraghi, H. Karimi-Maleh, A nanostructure voltammetric platform amplified with ionic liquid for determination of tert-butylhydroxyanisole in the presence kojic acid, J. Food Meas. Charact. 13 (2019)

1781–1787. https://doi.org/10.1007/s11694-019-00096-6.

[18] J. Ostojić, S. Herenda, Z. Bešić, M. Miloš, B. Galić, Advantages of an electrochemical method compared to the spectrophotometric kinetic study of peroxidase inhibition by boroxine derivative, Molecules. 22 (2017). https://doi.org/10.3390/molecules22071120.

[19] D. Galato, K. Ckless, M.F. Susin, C. Giacomelli, R.M. Ribeiro-do-Valle, a Spinelli, Antioxidant capacity of phenolic and related compounds: correlation among electrochemical, visible spectroscopy methods and structure-antioxidant activity., Redox Rep. 6 (2001) 243–50. https://doi.org/10.1179/135100001101536391.

[20] M.J. Rebelo, R. Rego, M. Ferreira, M.C. Oliveira, Comparative study of the antioxidant capacity and polyphenol content of Douro wines by chemical and electrochemical methods, Food Chem. 141 (2013) 566–573. https://doi.org/10.1016/j.foodchem.2013.02.120.

[21] J. Hoyos-Arbeláez, L. Blandón-Naranjo, M. Vázquez, J. Contreras-Calderón, Antioxidant capacity of mango fruit (Mangifera indica). An electrochemical study as an approach to the spectrophotometric methods, Food Chem. 266 (2018) 435–440. https://doi.org/10.1016/j.foodchem.2018.06.044.

[22] C.O. Chikere, N.H. Faisal, P. Kong Thoo Lin, C. Fernandez, The synergistic effect between graphene oxide nanocolloids and silicon dioxide nanoparticles for gallic acid sensing, J. Solid State Electrochem. 23 (2019) 1795–1809. https://doi.org/10.1007/s10008-019-04267-9.

[23] Y. Gao, L. Wang, Y. Zhang, L. Zou, G. Li, B. Ye, Highly sensitive determination of gallic acid based on a Pt nanoparticle decorated polyelectrolyte-functionalized graphene modified electrode, Anal. Methods. 8 (2016) 8474–8482.

https://doi.org/10.1039/c6ay02583h.

[24] C. Xiong, Y. Wang, H. Qu, L. Zhang, L. Qiu, W. Chen, F. Yan, L. Zheng, Highly sensitive detection of gallic acid based on organic electrochemical transistors with poly(diallyldimethylammonium chloride) and carbon nanomaterials nanocomposites functionalized gate electrodes, Sensors Actuators, B Chem. 246 (2017) 235–242. https://doi.org/10.1016/j.snb.2017.02.025.

[25] C. Chikere, N.H. Faisal, P.K.T. Lin, C. Fernandez, Zinc oxide nanoparticles modified-carbon paste electrode used for the electrochemical determination of Gallic acid, J. Phys. Conf. Ser. 1310 (2019) 012008. https://doi.org/10.1088/1742-6596/1310/1/012008.

[26] A. Puangjan, S. Chaiyasith, An efficient ZrO2/Co3O4/reduced graphene oxide nanocomposite electrochemical sensor for simultaneous determination of gallic acid, caffeic acid and protocatechuic acid natural antioxidants, Electrochim. Acta. 211 (2016) 273–288. https://doi.org/10.1016/j.electacta.2016.04.185.

[27] H. Karimi-Maleh, M. Sheikhshoaie, I. Sheikhshoaie, M. Ranjbar, J. Alizadeh, N.W. Maxakato, A. Abbaspourrad, A novel electrochemical epinine sensor using amplified CuO nanoparticles and a: N -hexyl-3-methylimidazolium hexafluorophosphate electrode, New J. Chem. 43 (2019) 2362–2367. https://doi.org/10.1039/c8nj05581e.

[28] M. Miraki, H. Karimi-Maleh, M.A. Taher, S. Cheraghi, F. Karimi, S. Agarwal, V.K. Gupta, Voltammetric amplified platform based on ionic liquid/NiO nanocomposite for determination of benserazide and levodopa, J. Mol. Liq. 278 (2019) 672–676. https://doi.org/10.1016/j.molliq.2019.01.081.

[29] F. Tahernejad-Javazmi, M. Shabani-Nooshabadi, H. Karimi-Maleh, 3D reduced graphene oxide/FeNi3-ionic liquid nanocomposite modified sensor; an electrical

synergic effect for development of tert-butylhydroquinone and folic acid sensor, Compos. Part B Eng. 172 (2019) 666–670. https://doi.org/10.1016/j.compositesb.2019.05.065.

[30] H. Karimi-Maleh, C.T. Fakude, N. Mabuba, G.M. Peleyeju, O.A. Arotiba, The determination of 2-phenylphenol in the presence of 4-chlorophenol using nano-Fe3O4/ionic liquid paste electrode as an electrochemical sensor, J. Colloid Interface Sci. 554 (2019) 603–610. https://doi.org/10.1016/j.jcis.2019.07.047.

[31] H. Karimi-Maleh, O.A. Arotiba, Simultaneous determination of cholesterol, ascorbic acid and uric acid as three essential biological compounds at a carbon paste electrode modified with copper oxide decorated reduced graphene oxide nanocomposite and ionic liquid, J. Colloid Interface Sci. 560 (2020) 208–212. https://doi.org/10.1016/j.jcis.2019.10.007.

[32] M. Bijad, H. Karimi-Maleh, M. Farsi, S.A. Shahidi, An electrochemical-amplified-platform based on the nanostructure voltammetric sensor for the determination of carmoisine in the presence of tartrazine in dried fruit and soft drink samples, J. Food Meas. Charact. 12 (2018) 634–640. https://doi.org/10.1007/s11694-017-9676-1.

[33] F. Tahernejad-Javazmi, M. Shabani-Nooshabadi, H. Karimi-Maleh, Analysis of glutathione in the presence of acetaminophen and tyrosine via an amplified electrode with MgO/SWCNTs as a sensor in the hemolyzed erythrocyte, Talanta. 176 (2018) 208–213. https://doi.org/10.1016/j.talanta.2017.08.027.

[34] O.E. Fayemi, A.S. Adekunle, Metal Oxide Nanoparticles/Multi-walled Carbon Nanotube Nanocomposite Modified Electrode for the Detection of Dopamine: Comparative Electrochemical Study, J. Biosens. Bioelectron. 06 (2015) 190. https://doi.org/10.4172/2155-6210.1000190.

[35] J. Tashkhourian, S.F.F. Nami-Ana, A sensitive electrochemical sensor for determination of gallic acid based on SiO2nanoparticle modified carbon paste electrode, Mater. Sci. Eng. C. 52 (2015) 103–110. https://doi.org/10.1016/j.msec.2015.03.017.

[36] C.O. Chikere, N.H. Faisal, P. Kong-Thoo-Lin, C. Fernandez, Interaction between Amorphous Zirconia Nanoparticles and Graphite: Electrochemical Applications for Gallic Acid Sensing Using Carbon Paste Electrodes in Wine, Nanomaterials. 10 (2020) 537. https://doi.org/10.3390/nano10030537.

[37] E. Mehmeti, D.M. Stanković, S. Chaiyo, Ľ. Švorc, K. Kalcher, Manganese dioxide-modified carbon paste electrode for voltammetric determination of riboflavin, Microchim. Acta. 183 (2016) 1619–1624. https://doi.org/10.1007/s00604-016-1789-4.

[38] Y. Zhao, S. Chen, B. Sun, D. Su, X. Huang, H. Liu, Y. Yan, K. Sun, G. Wang, Graphene-Co3O4 nanocomposite as electrocatalyst with high performance for oxygen evolution reaction, Sci. Rep. (2015). https://doi.org/10.1038/srep07629.

[39] Z.-Y. Li, P.T.M. Bui, D.-H. Kwak, M.S. Akhtar, O.-B. Yang, Enhanced electrochemical activity of low temperature solution process synthesized Co3O4 nanoparticles for pseudo-supercapacitors applications, Ceram. Int. 42 (2016) 1879–1885. https://doi.org/10.1016/J.CERAMINT.2015.09.155.

[40] Y.I. Choi, H.J. Yoon, S.K. Kim, Y. Sohn, Crystal-facet dependent CO oxidation, preferential oxidation of CO in H2-rich, water-gas shift reactions, and supercapacitor application over Co3O4 nanostructures, Appl. Catal. A Gen. 519 (2016) 56–67. https://doi.org/10.1016/J.APCATA.2016.03.027.

[41] K.F. Wadekar, Nemade K.R., Waghuley S.A., Chemical synthesis of cobalt oxide (Co3O4) nanoparticles using Co-precipitation method, Res. J. Chem. Int. Sci.

Community Assoc. Res. J. Chem. Sci. Res. J. Chem. Sci. 7 (2017) 53–55. https://doi.org/10.1051/jp4:2001380.

[42] J. Yang, H. Liu, W.N. Martens, R.L. Frost, Synthesis and characterization of Cobalt hydroxide, cobalt oxyhydroxide, and cobalt oxide nanodiscs, J. Phys. Chem. C. 114 (2010) 111–119. https://doi.org/10.1021/jp908548f.

[43] N. Rani, G. Rani, M. Kumar, Green synthesis , characterization and optical properties of cobalt oxide nanoparticles by co-precipitation method, Int. J. Adv. Res. Dev. 3 (2018) 1195–1198.

[44] L. Estepa, M. Daudon, Contribution of Fourier transform infrared spectroscopy to the identification of urinary stones and kidney crystal deposits, Biospectroscopy. 3 (1997) 347–369.

[45] F. Chekin, S.M. Vahdat, M.J. Asadi, Green synthesis and characterization of cobalt oxide nanoparticles and its electrocatalytic behavior, Russ. J. Appl. Chem. 89 (2016) 816–822. https://doi.org/10.1134/S1070427216050219.

[46] J. Tashkhourian, S.F. Nami-Ana, A sensitive electrochemical sensor for determination of gallic acid based on SiO2nanoparticle modified carbon paste electrode, Mater. Sci. Eng. C. 52 (2015) 103–110. https://doi.org/10.1016/j.msec.2015.03.017.

[47] J.H. Luo, B.L. Li, N.B. Li, H.Q. Luo, Sensitive detection of gallic acid based on polyethyleneimine- functionalized graphene modified glassy carbon electrode, Sensors Actuators, B Chem. 186 (2013) 84–89. https://doi.org/10.1016/j.snb.2013.05.074.

[48] J. Tashkhourian, S.F.N. Ana, S. Hashemnia, M.R. Hormozi-Nezhad, Construction of a modified carbon paste electrode based on TiO2 nanoparticles for the determination of gallic acid, J. Solid State Electrochem. 17 (2013) 157–165.

https://doi.org/10.1007/s10008-012-1860-y.

[49] I. Novak, M. Šeruga, Š. Komorsky-Lovrić, Electrochemical characterization of epigallocatechin gallate using square-wave voltammetry, Electroanalysis. 21 (2009) 1019–1025. https://doi.org/10.1002/elan.200804509.

[50] L.P. Souza, F. Calegari, A.J.G. Zarbin, L.H. Marcolino-Júnior, M.F. Bergamini, Voltammetric Determination of the Antioxidant Capacity in Wine Samples Using a Carbon Nanotube Modified Electrode, J. Agric. Food Chem. 59 (2011) 7620–7625. https://doi.org/10.1021/jf2005589.

[51] A.E. Fazary, M. Taha, Y.H. Ju, Iron complexation studies of gallic acid, J. Chem. Eng. Data. 54 (2009) 35–42. https://doi.org/10.1021/je800441u.

[52] P. a Kilmartin, H. Zou, A.L. Waterhouse, A Cyclic Voltammetry Method Suitable for Characterizing Antioxidant Properties of Wine and Wine Phenolics A Cyclic Voltammetry Method Suitable for Characterizing Antioxidant Properties of Wine and Wine Phenolics, J. Agric. Food Chem. 49 (2001) 1957–1965. https://doi.org/10.1021/jf001044u.

[53] O. Makhotkina, P.A. Kilmartin, Uncovering the influence of antioxidants on polyphenol oxidation in wines using an electrochemical method: Cyclic voltammetry, J. Electroanal. Chem. 633 (2009) 165–174. https://doi.org/10.1016/j.jelechem.2009.05.007.

[54] M. López-Vélez, F. Martínez-Martínez, C. Del Valle-Ribes, The Study of Phenolic Compounds as Natural Antioxidants in Wine, Crit. Rev. Food Sci. Nutr. 43 (2003) 233–244. https://doi.org/10.1080/727072831.

[55] A. Ragusa, C. Centonze, M.E. Grasso, M.F. Latronico, P.F. Mastrangelo, F. Sparascio,

M. Maffia, HPLC analysis of phenols in Negroamaro and primitivo red wines from salento, Foods. 8 (2019) 45. https://doi.org/10.3390/foods8020045.

Electroanalytical determination of gallic acid in Red and White wine samples using Cobalt Oxide Nanoparticles-modified carbon-paste electrodes

Chrys. O. CHIKERE[a], Emma HOBBEN[a], Nadimul Haque FAISAL[b], Paul KONG-THOO-LIN[a], Carlos FERNANDEZ[a*]

a. *School of Pharmacy and Life Sciences, the Robert Gordon University, Aberdeen, AB10 7GJ, United Kingdom*

b. *School of Engineering, the Robert Gordon University, Aberdeen AB10 7GJ, United Kingdom*

** Corresponding Author. Tel. +44 (0) 1224 262559 E-mail: c.fernandez@rgu.ac.uk*

LIST OF FIGURES

Fig 1. (a) The SEM Image of Cobalt oxide nanoparticles showing the morphology of the nanoparticles with (Inset) Co_3O_4 in 100 nm **(b)** SEM Image of CoO-nano-CPE, with the paraffin holding the Cobalt oxide nanoparticles and graphite together **(c)** EDXA analysis of Cobalt oxide nanoparticles **(d)** Size distribution of cobalt oxide nanoparticles using a Zetasizer..

Fig 2. (a) Cyclic voltammetry of GA (10 mmol L^{-1}) at the CoO-NPs-CPE and bare CPE in 1 x 10^2 mmol L^{-1} phosphate buffer of pH 2.0 at a scan rate of 100 mVs^{-1}. **(b)** The cyclic voltammograms of 5 mmol L^{-1} $[Fe(CN)_6]^{3-/4-}$ redox solution, using bare CPE and CoO-NPs-CPE, **(c)** Nyquist plot showing the EIS measurements of $[Fe(CN)_6]^{3-/4-}$ (5 mmol L^{-1}) using the bare CPE and CoO-NPs-CPE (inset) The equivalent circuit used for the calculation.

Fig 3. Cyclic voltammograms of 10 mmol L^{-1} GA at Co_3O_4 nanoparticles-modified CPE, bulk Co_3O_4 nanoparticles-modified CPE and bare CPE in 1 x 10^2 mmol L^{-1} phosphate buffer of pH 2.0 at a scan rate of 100 mVs^{-1}

Fig 4. (a) Differential voltammograms of various concentrations of GA at CoO-nano-CPE in a 1 x 10^{-2} mmol L^{-1} phosphate buffer at pH 2.0 at scan rate of 100 mVs^{-1}, with voltammograms (a-j) that corresponds to the following concentrations a) Blank PBS, b) 1 x 10^{-4} mmol L^{-1}, c) 2.5 x 10^{-4} mmol L^{-1}, d) 5 x 10^{-4} mmol L^{-1}, e) 7.5 x 10^{-4} mmol L^{-1}, f) 1 x 10^{-3} mmol L-1, g) 2.5 x 10^{-3} mmol L^{-1}, h) 5 x 10^{-3} mmol L^{-1}, i) 7.5 x 10^{-3} mmol L^{-1}, j) 1 x 10^{-2} mmol L^{-1} (inset) Plot of concentration of GA against peak currents. **(b)** The plot of the Peak Current (I_p) against the concentration of GA, showing the effect of

concentration on the electrochemical behaviour of increasing GA concentration, using CoO-nano-CPE at a scan rate of 100 mVs^{-1}

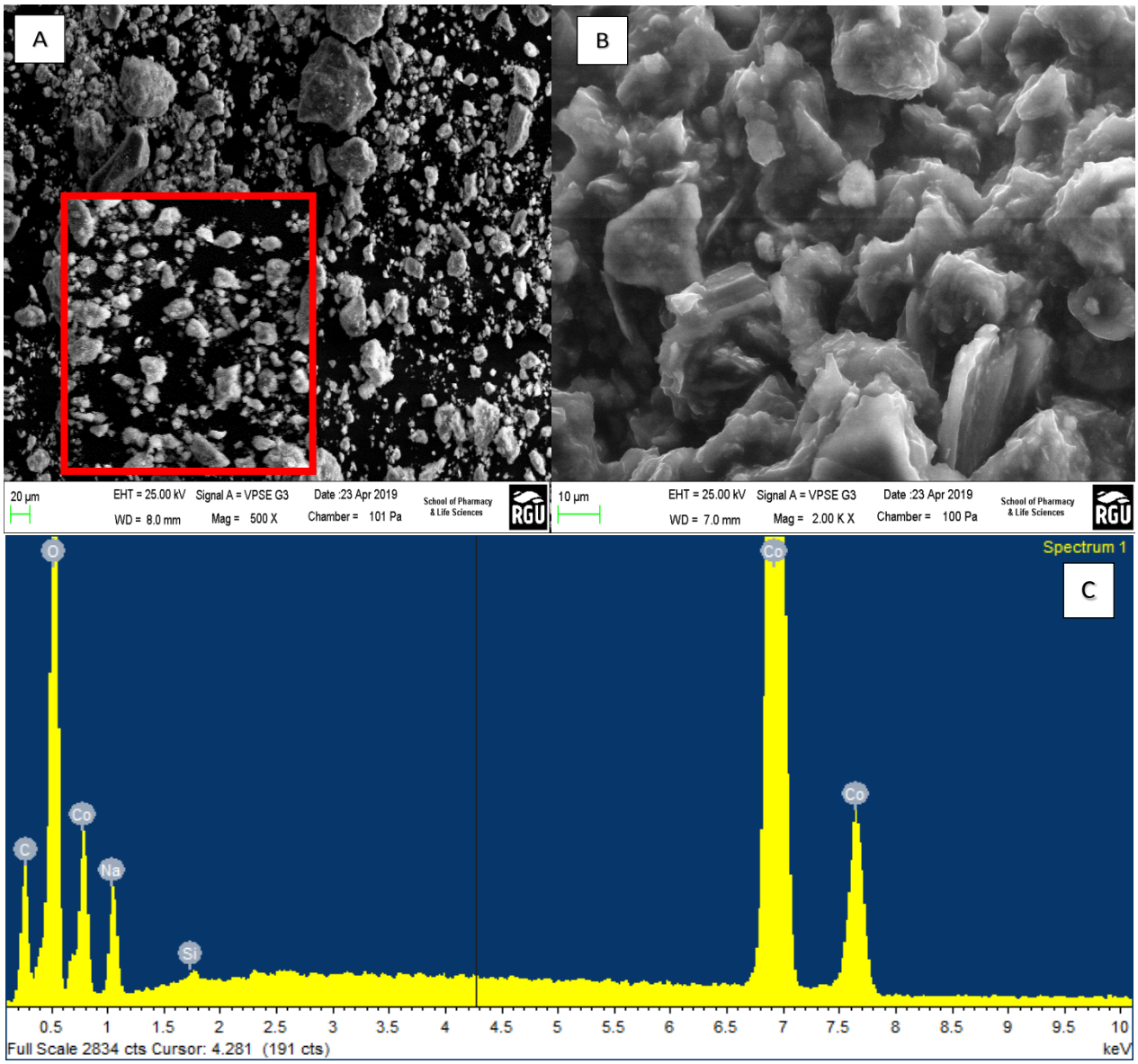

Results

			Size (d.nm):	% Intensity:	St Dev (d.n...
Z-Average (d.nm):	279.4	Peak 1:	288.2	83.3	144.5
PdI:	0.250	Peak 2:	1835	16.7	871.6
Intercept:	0.909	Peak 3:	0.000	0.0	0.000
Result quality :	Good				

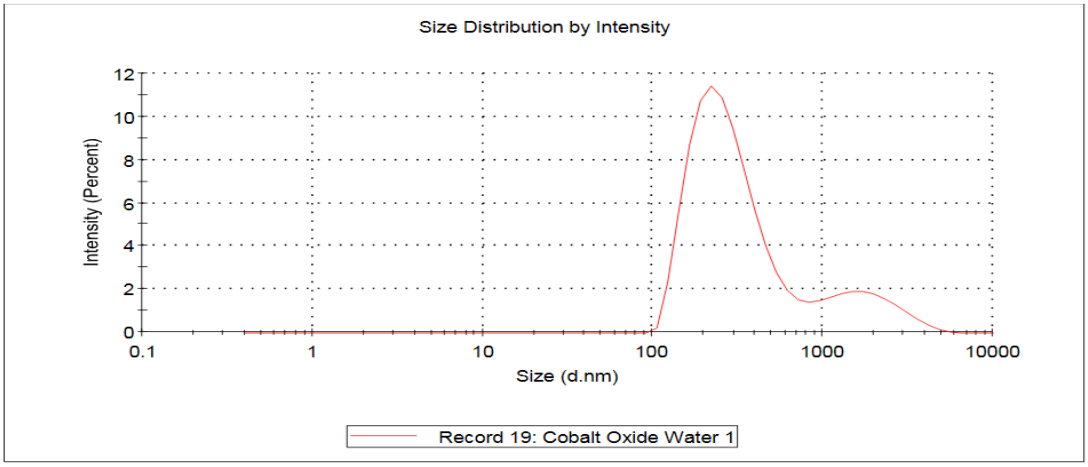

Fig 1. (a) The SEM Image of Cobalt oxide nanoparticles showing the morphology of the nanoparticles with (Inset) Co_3O_4 in 100 nm (**b)** SEM Image of CoO-nano-CPE, with the paraffin holding the Cobalt oxide nanoparticles and graphite together **(c)** EDXA analysis of Cobalt oxide nanoparticles **(d)** Size distribution of cobalt oxide nanoparticles using a Zetasizer.

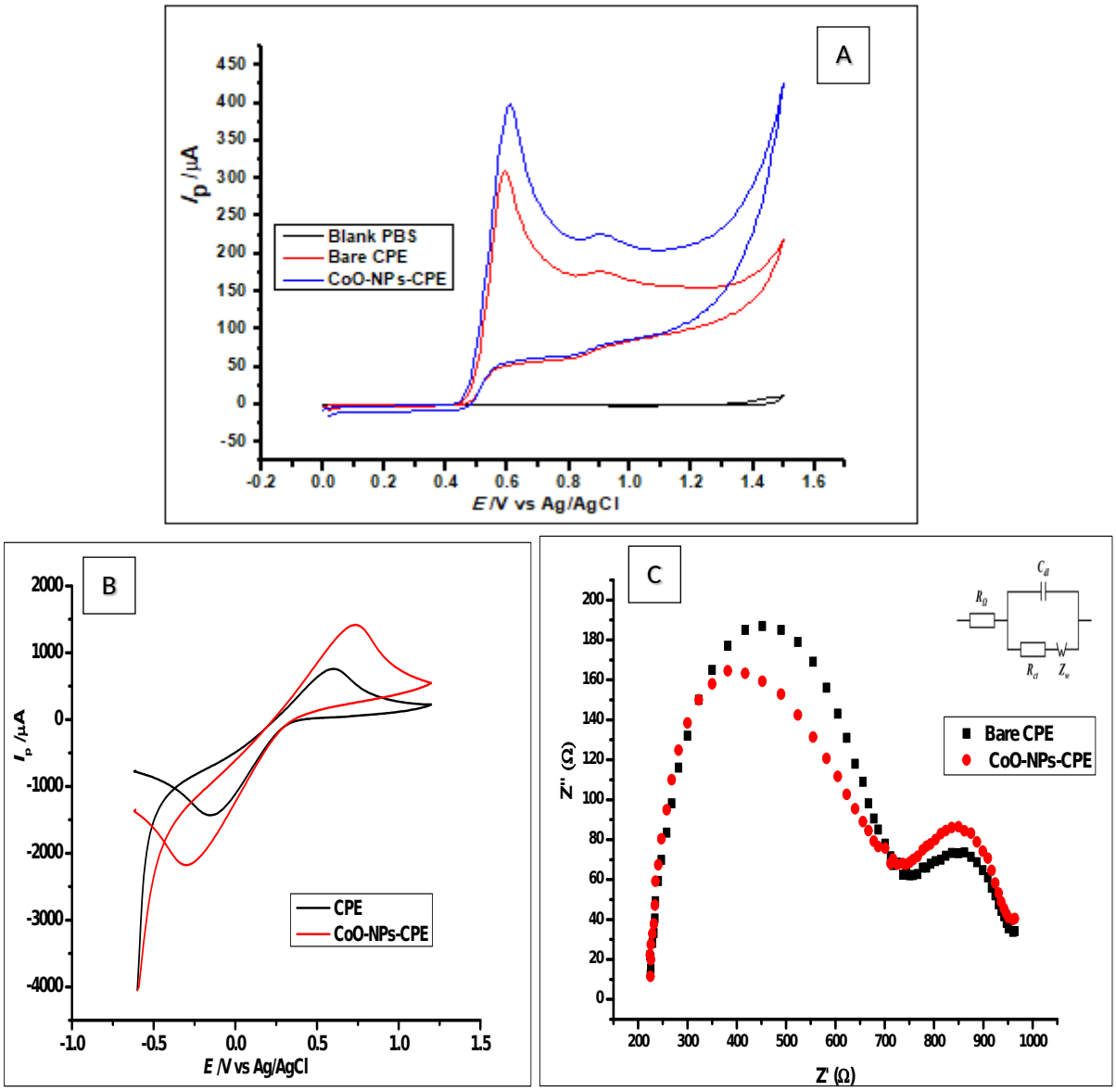

Fig 2. (a) Cyclic voltammetry of GA (10 mmol L^{-1}) at the CoO-NPs-CPE and bare CPE in 1 x 10^2 mmol L^{-1} phosphate buffer of pH 2.0 at a scan rate of 100 mVs^{-1}. **(b)** The cyclic voltammograms of 5 mmol L^{-1} $[Fe(CN)_6]^{3-/4-}$ redox solution, using bare CPE and CoO-NPs-CPE, **(c)** Nyquist plot showing the EIS measurements of $[Fe(CN)_6]^{3-/4-}$ (5 mmol L^{-1}) using the bare CPE and CoO-NPs-CPE (inset) The equivalent circuit used for the calculation.

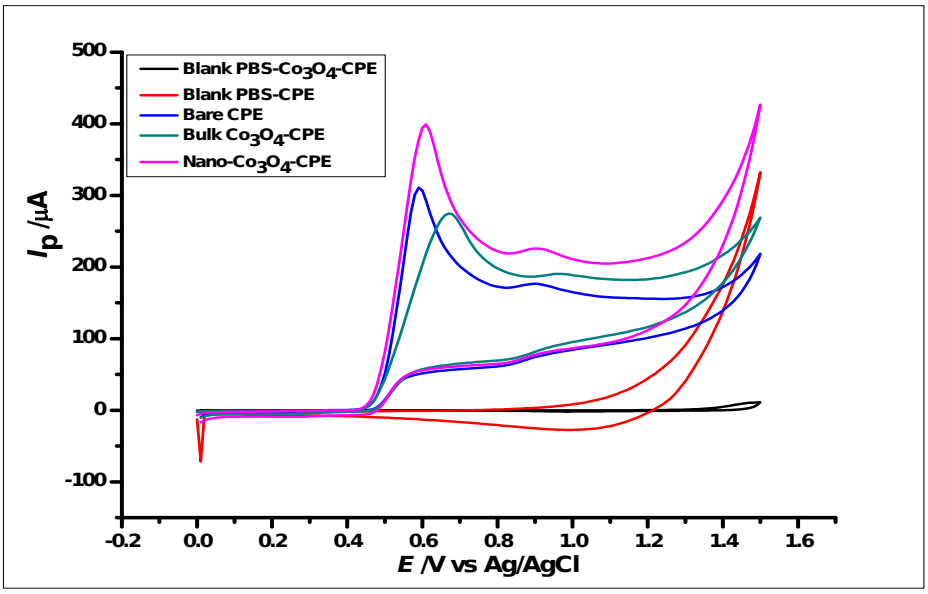

Fig 3. Cyclic voltammograms of 10 mmol L^{-1} GA at Co_3O_4 nanoparticles-modified CPE, bulk Co_3O_4 nanoparticles-modified CPE and bare CPE in 1 x 10^2 mmol L^{-1} phosphate buffer of pH 2.0 at a scan rate of 100 mVs^{-1}

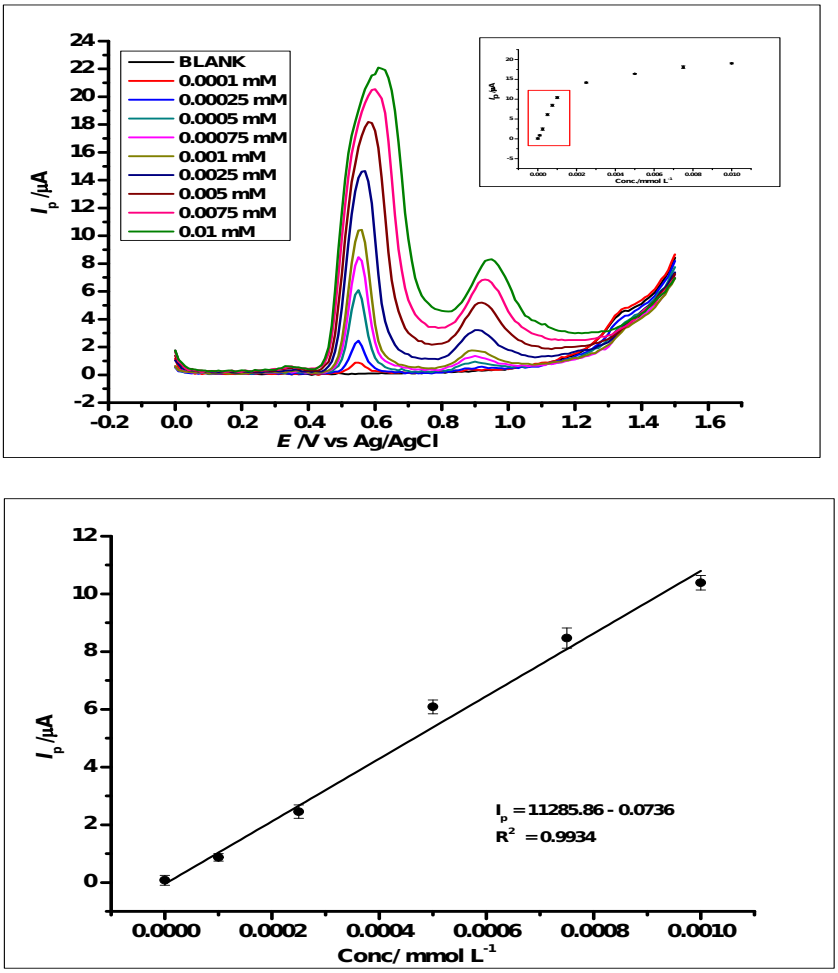

Fig 4. (a) Differential voltammograms of various concentrations of GA at CoO-nano-CPE in a 0.1 mol L^{-1} phosphate buffer at pH 2.0 at scan rate of 100 mVs^{-1}, with voltammograms (a-j) that corresponds to the following concentrations a) Blank PBS, b) 1 x 10^{-4} mmol L^{-1}, c) 2.5 x 10^{-4} mmol L^{-1}, d) 5 x 10^{-4} mmol L^{-1}, e) 7.5 x 10^{-4} mmol L^{-1}, f) 1 x 10^{-3} mmol L^{-1}, g) 2.5 x 10^{-3} mmol L^{-1}, h) 5 x 10^{-3} mmol L^{-1}, i) 7.5 x 10^{-3} mmol L^{-1}, j) 1 x 10^{-2} mmol L^{-1} (inset) Plot of concentration of GA against peak currents. **(b)** The plot of the Peak Current (I_p) against the concentration of GA, showing the effect of concentration on the electrochemical behaviour of increasing GA concentration, using CoO-nano-CPE at a scan rate of 100 mVs^{-1}

Electroanalytical determination of gallic acid in Red and White wine samples using Cobalt Oxide Nanoparticles-modified carbon-paste electrodes

Chrys. O. CHIKERE[a], Emma HOBBEN[a], Nadimul Haque FAISAL[b], Paul KONG-THOO-LIN[a], Carlos FERNANDEZ[a*]

a. *School of Pharmacy and Life Sciences, the Robert Gordon University, Aberdeen, AB10 7GJ, United Kingdom*

b. *School of Engineering, the Robert Gordon University, Aberdeen AB10 7GJ, United Kingdom*

** Corresponding Author. Tel. +44 (0) 1224 262559 E-mail: c.fernandez@rgu.ac.uk*

List of tables

Table 1. The absorbance values of GA (1 x 10^{-3} mol L^{-1}) at different pH at the wavelength of 280nm

	pH Values	Absorbance (Wavelength 280 nm)
1	2.0	2.205 ± 0.02
2	4.0	3.09 ± 0.02
3	6.0	3.52 ± 0.06
4	8.0	33.92 ± 0.6
5	10	37.49 ± 0.15

Table 2. Metal Oxide Nanoparticles (MO-NPs) and Metal Nanoparticles composites in different electrochemical sensor systems for the determination of Gallic acid.

	Electrodes	Method	Medium Analysed	Linear Range (mol L^{-1})	Limit of Detection (mol L^{-1})	Reference
1	ZnO-NPs-CPE	CV, DPV	Red Wine	1 x 10^{-6} – 5 x 10^{-5}	1.86 x 10^{-7}	[25]
2	SiO_2-NPs -GrO nanocolloids-GCE	CV, DPV	Red and White wine	6.25 x 10^{-6} to 1 x 10^{-3}	2.09 x 10^{-6}	[22]

3	Amorphous Zirconia-CPE	CV, DPV	Red and White Wine	1×10^{-6} – 1×10^{-3}	1.24×10^{-7}	[36]
4	ZrO_2/Co_3O_4/rGO-FTO	CV, DPV	Fruit juice, Tea	6.24×10^{-9} – 4.8×10^{-7}	1.56×10^{-9}	[26]
5	Bismuth-NPs-MWCNT-CPE	CV, Amperometry	Clove and Green Tea	1×10^{-6} – 1×10^{-4}	1.6×10^{-7}	[14]
6	TiO_2-NPs-CPE	CV, DPV	Green and Black Tea	2.5×10^{-6} - 1.5×10^{-4}	9.4×10^{-7}	[48]
7	CoO-NPs-CPE	CV, DPV	Red and White Wine	1×10^{-4} to 1×10^{-2}	1.52×10^{-6}	This Work

Table 3. Results of the analysis of GA in spiked Red Wine and White Wine

	Australian Wine			
Sample	**Added (mmol L^{-1})**	**Found (mmol L^{-1})**	**Relative Error**	**Recovery (%)**
Red Wine	0.0	0.688	-	-
	0.9	0.787	±13	87
	1.6	1.599	±0.7	99.93
	2.31	2.35	±1.73	101.73
White Wine	0.0	0.076	-	-
	0.9	0.995	±10.5	110.5
	1.6	1.658	±3.63	103.63
	2.31	2.23	±3.46	96.54
	United States of America Wine			
	Added (mmol L^{-1})	**Found (mmol L^{-1})**	**Relative Error**	**Recovery (%)**
Red Wine	0.0	0.844	-	-
	0.9	0.931	±3.4	103.4
	1.6	1.501	±6.19	93.81
	2.31	2.33	±0.87	100.87
White Wine	0.0	0.0083	-	-
	0.9	0.911	±1.2	101.2
	1.6	1.582	±1.12	98.88
	2.31	2.271	±1.69	98.31

Conflict of interest

Dr. Chrys. O. Chikere declares that he has no conflict of interest. Ms. Emma Hobben declares that she has no conflict of interest. Dr. Nadimul H Faisal declares that he has no conflict of interest. Professor Paul Kong-Thoo-Lin declares that he has no conflict of interest. Dr. Carlos Fernandez declares that he has no conflict of interest.

Electroanalytical determination of gallic acid in Red and White wine samples using Cobalt Oxide Nanoparticles-modified carbon-paste electrodes

Chrys. O. CHIKERE[a], Emma HOBBEN[a], Nadimul Haque FAISAL[b], Paul Kong THOO-LIN[a], Carlos FERNANDEZ[a*]

a. *School of Pharmacy and Life Sciences, the Robert Gordon University, Aberdeen, AB10 7GJ, United Kingdom*

b. *School of Engineering, the Robert Gordon University, Aberdeen AB10 7GJ, United Kingdom*

** Corresponding Author. Tel. +44 (0) 1224 262559 E-mail: c.fernandez@rgu.ac.uk*

Electronic Supplementary Material

S1 The FTIR Characterisation

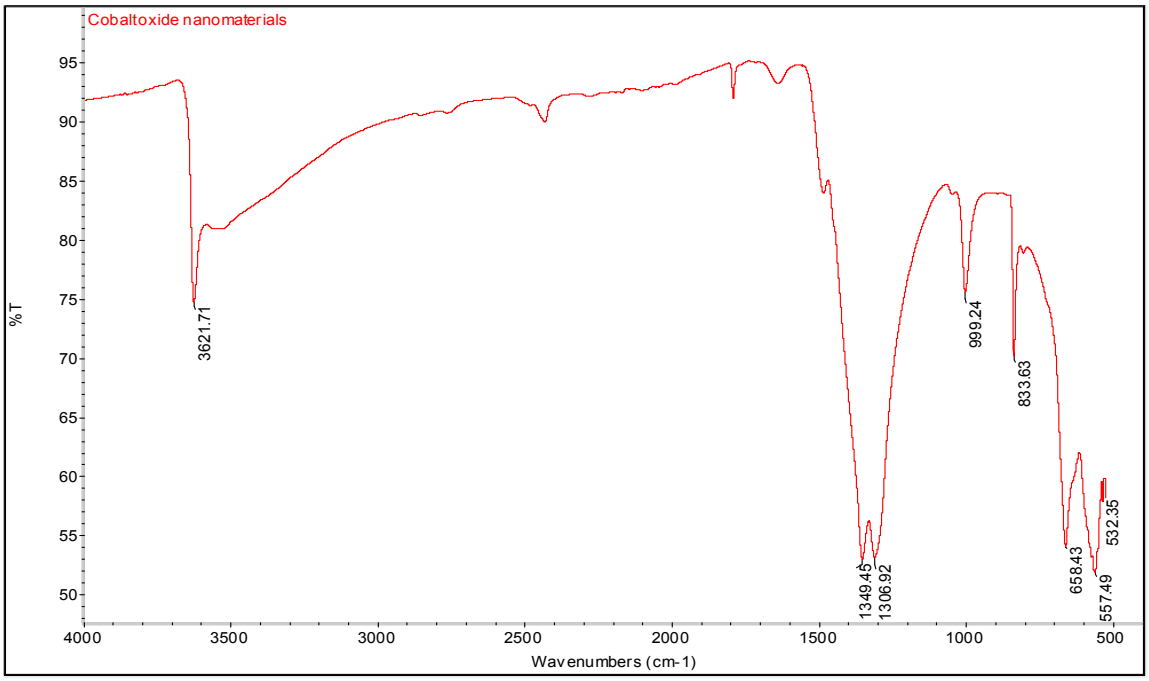

Fig. S1. FT-IR Image showing the spectra of Co_3O_4 nanoparticles

S2 The Thermogravimetric Analysis (TGA)

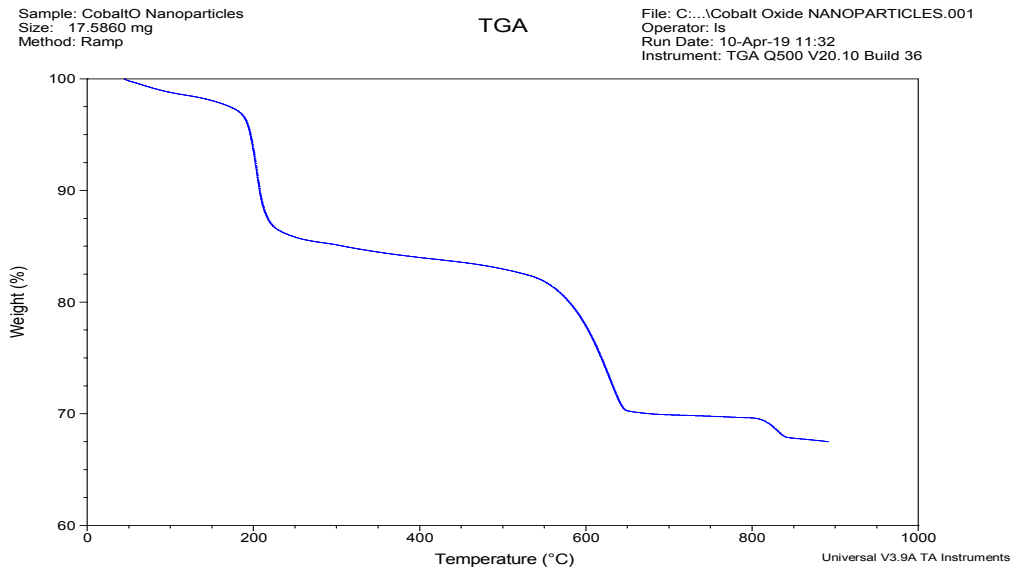

Fig S2. TGA result in the analysis of cobalt oxide nanoparticles

S3 Effective Surface Area Measurement

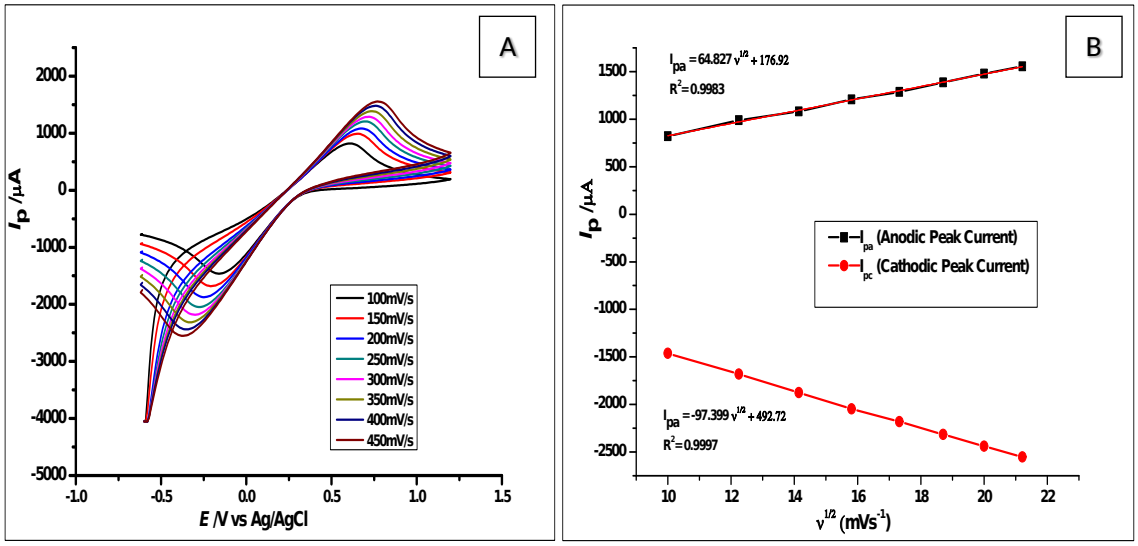

Fig. S3. (a) Cyclic voltammograms of $[Fe(CN)_6]^{3-/4-}$ (1 mmol L^{-1}) measured with CoO-NPs-CPE at increasing scan rates of 100-450 mVs^{-1} **(b)** Plots of I_p vs $v^{1/2}$ used for the calculation of the reactive surface area.

S4 The Reaction Mechanism of Gallic Acid oxidation

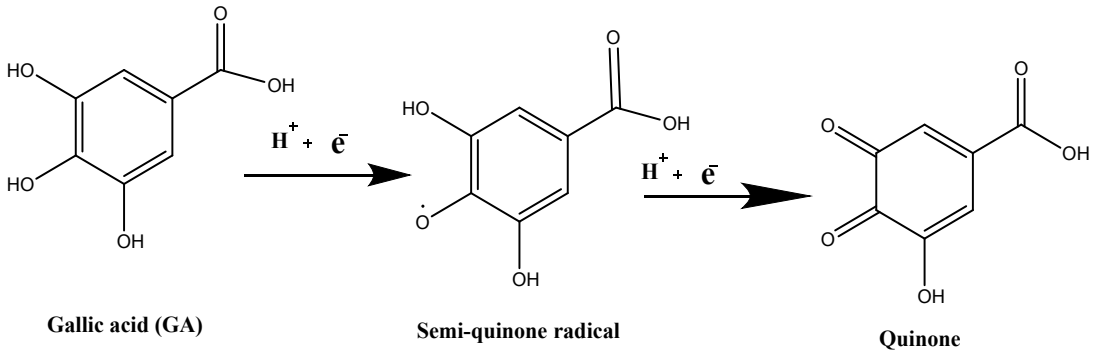

Gallic acid (GA) | Semi-quinone radical | Quinone

Fig. S4. The reaction mechanism of the oxidation of Gallic acid, showing the two peaks (semiquinone radical and the quinone)

S5 Effect of pH on Gallic acid Oxidation

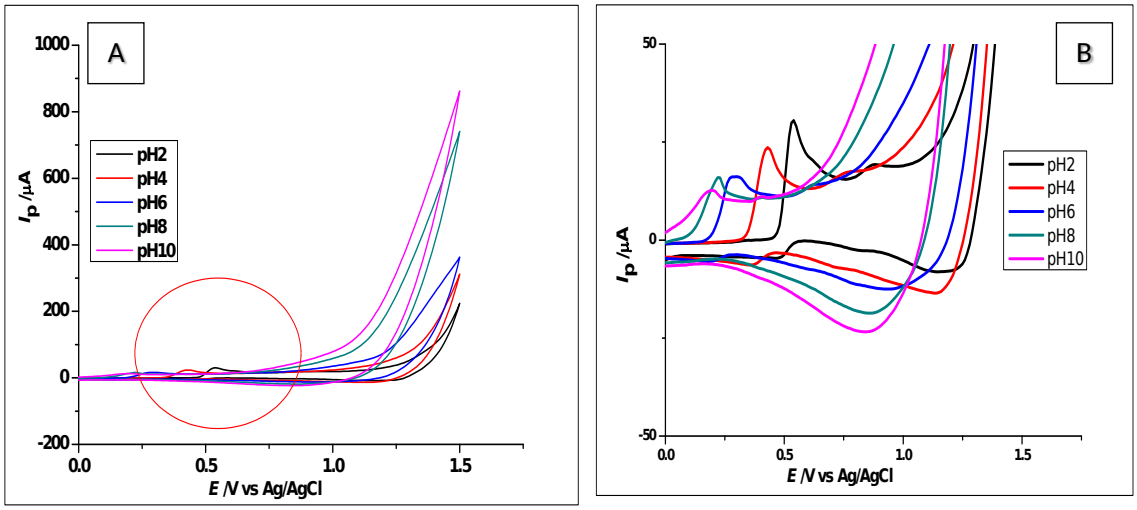

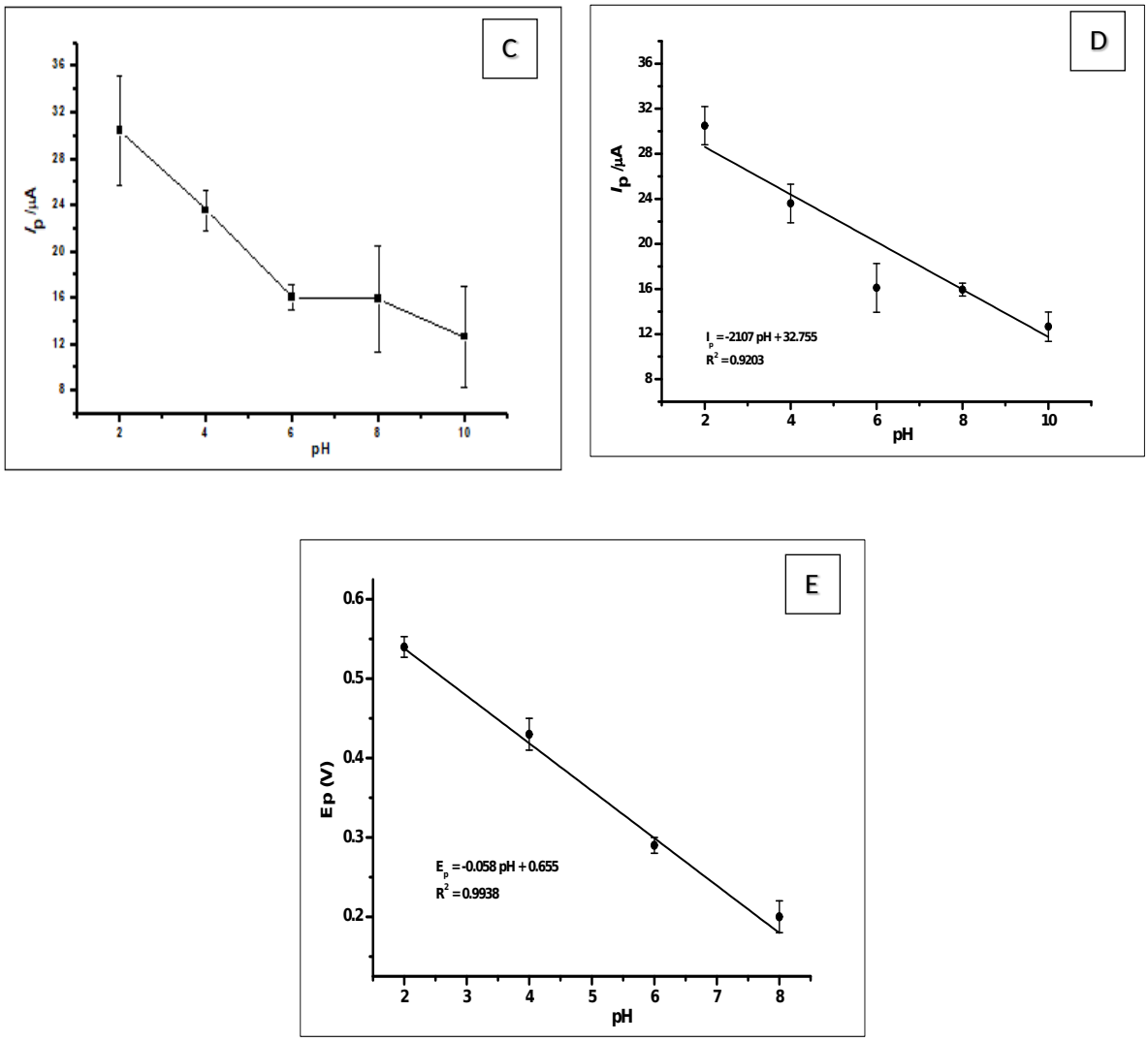

Fig. S5 (a) Cyclic voltammograms of 1 x 10^{-3} mol L^{-1} GA in the different pH range of 2.0 to 10.0 at a scan rate 100 mVs^{-1} **(b)** Zoomed section of the voltammograms **(c)** A graph of pH against the peak currents **(d)** Non-linear plot of peak current (I_p) vs pH **(e)** Linear plot of peak potential (E_p) vs pH

S6. Colour changes of GA solutions at different pH

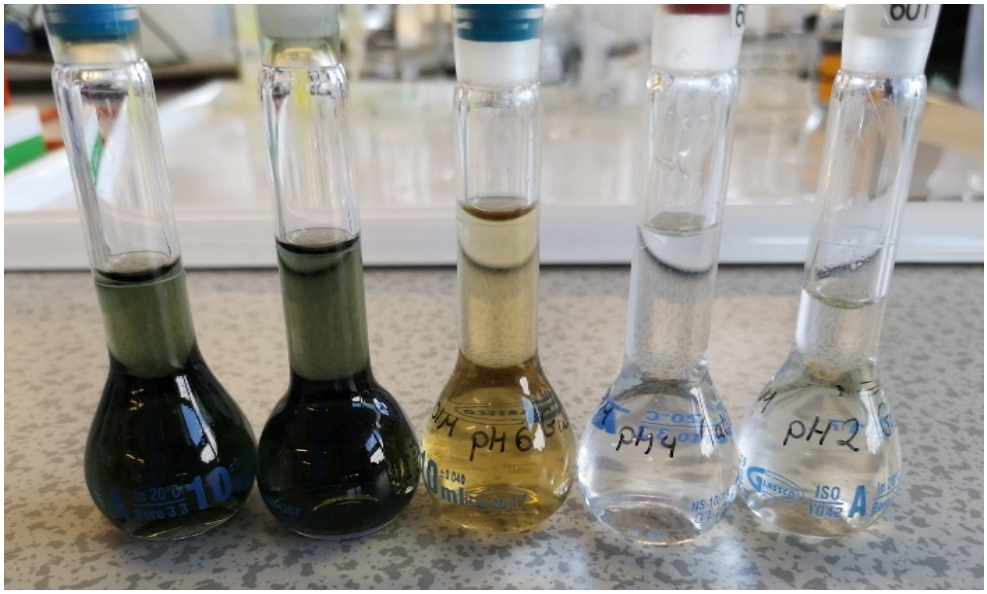

Fig. S6. Images of Gallic acid solutions at different pH, showing a very dark solution at a pH 10, that becomes brighter as the pH reduces to pH 8 to pH 2.

S7. Effect of Scan rate on Gallic acid oxidation

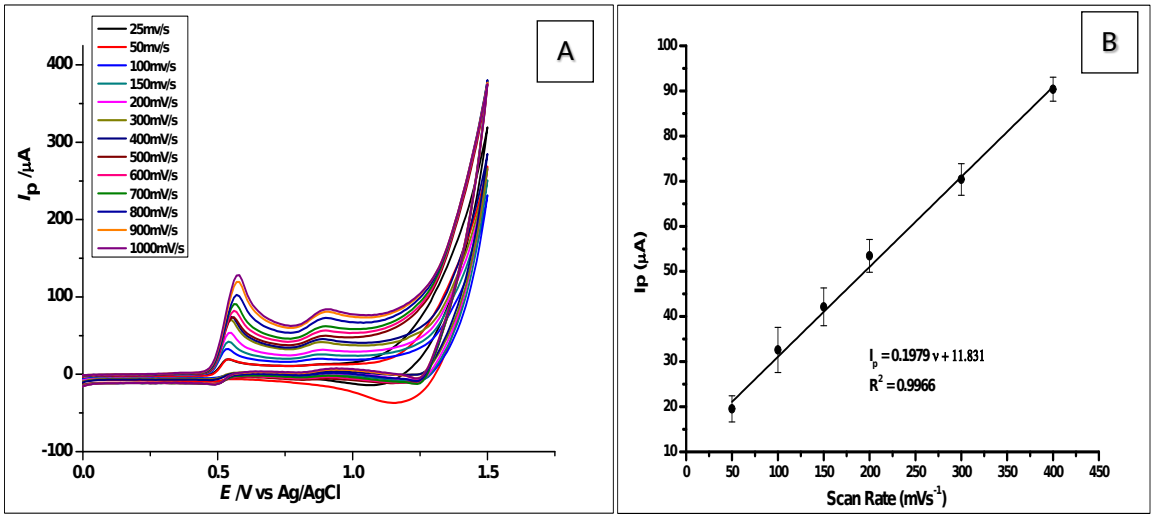

Fig. S7 (a) CV voltammograms of 1 x 10^{-3} mol L^{-1} GA in 1 x 10^{-1} mol L^{-1} Phosphate buffer solution at pH 2.0, showing different scan rates ranging from 50 -1000 mVs^{-1} **(b)** Plot of the scan rates from 50-400 mVs^{-1} against the peak current.

S8. Effect of Cobalt Oxide nanoparticles concentration on the CPE mixture

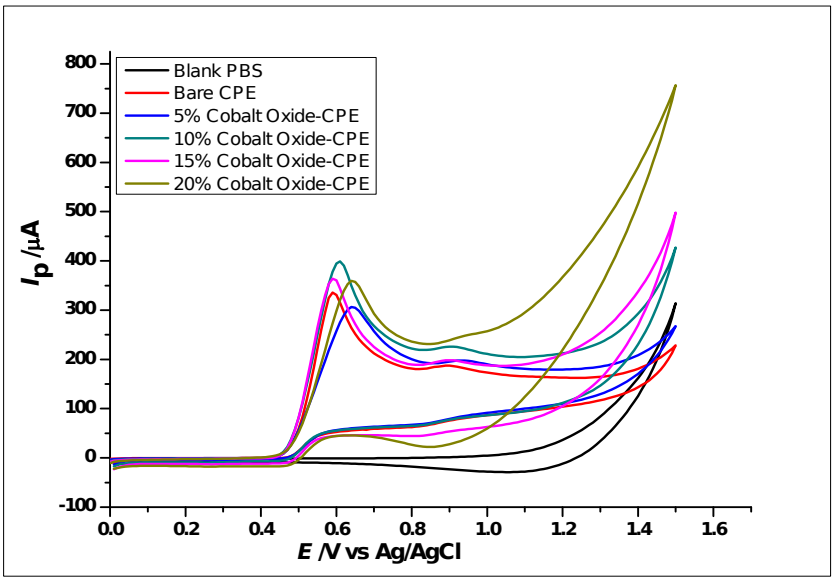

Fig.S8 Voltammograms showing changes in the constitution of the carbon paste electrode using 5%, 10%, 15% and 20% Cobalt oxide nanoparticles constituted in the modified CPE. This was used to determine 1 x 10^{-2} mol L^{-1} GA in 1 x 10^{-1} mol L^{-1} phosphate buffer at pH 2.0 using CV at a scan rate of 100 mVs^{-1}

S9 Reproducibility and repeatability of the method

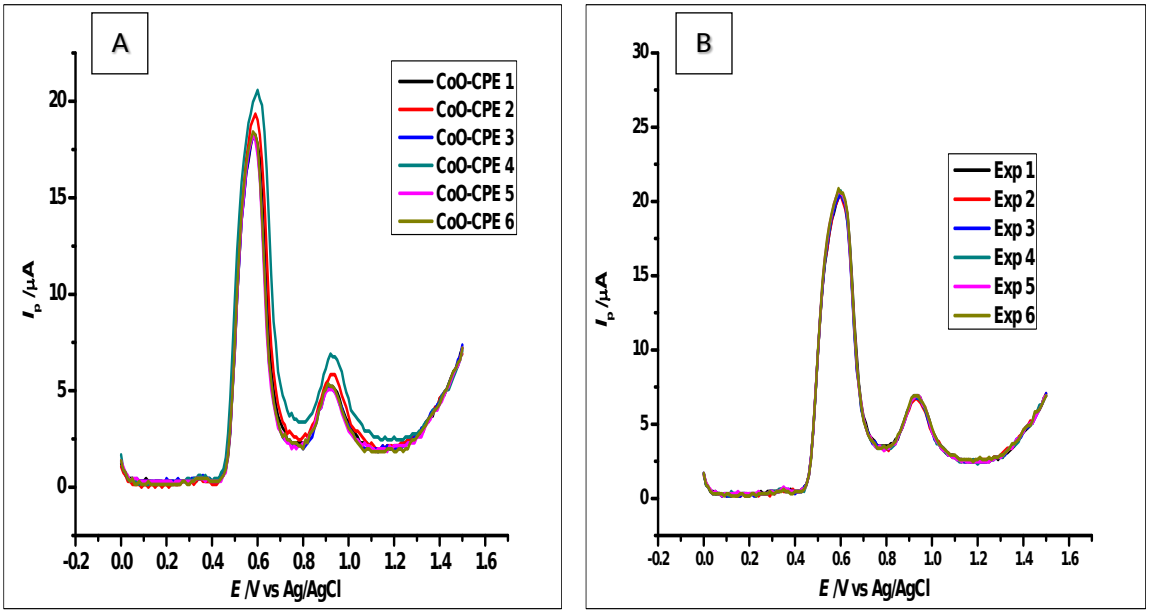

Fig. S9 DPV voltammograms of 5 x 10^{-4} mol L^{-1} Gallic acid showing **(a)** Reproducibility of the CoO nanoparticles modified CPE **(b)** Repeatability of the CoO nanoparticles modified CPE

S10 Stability of the method

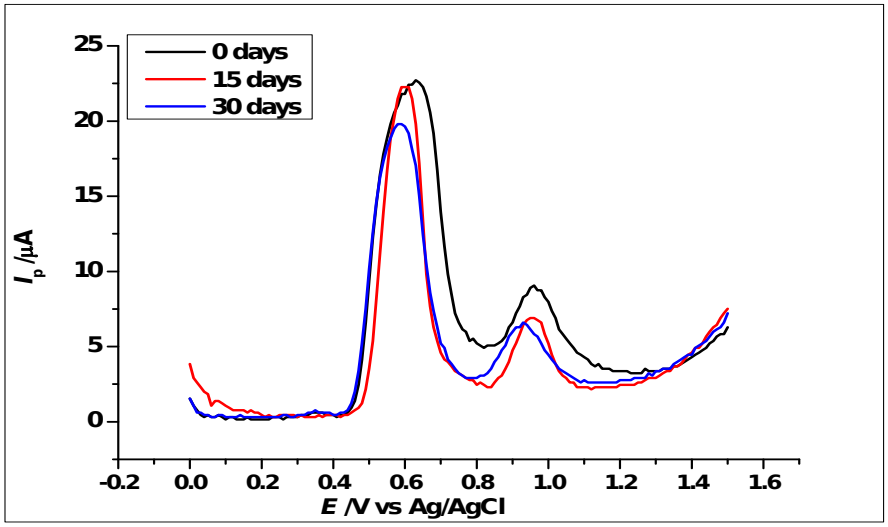

Fig. S10. DPV voltammograms of 5 x 10^{-4} mol L^{-1} Gallic acid, showing voltammograms measured by the same electrodes after 0 days, 15 days and 30 days: showing stability.

S11. Interference Study

Table S2. Effects of various foreign species on the determination of GA (1 x 10^{-2} mol L^{-1})

	Interfering Species and Ions	Concentration (mol L^{-1})	Relative Standard Deviation (%)
1	K^+	1 x 10^{-1}	±2.54
2	Cl^-	1 x 10^{-1}	±2.77
3	Na^+	1 x 10^{-1}	±4.51
4	Fe^{3+}	1 x 10^{-1}	±0.61
5	Ascorbic Acid	1 x 10^{-3}	±3.7
6	Quercetin	1 x 10^{-3}	±4.16

S12. Voltammograms of GA determination in Wine Samples

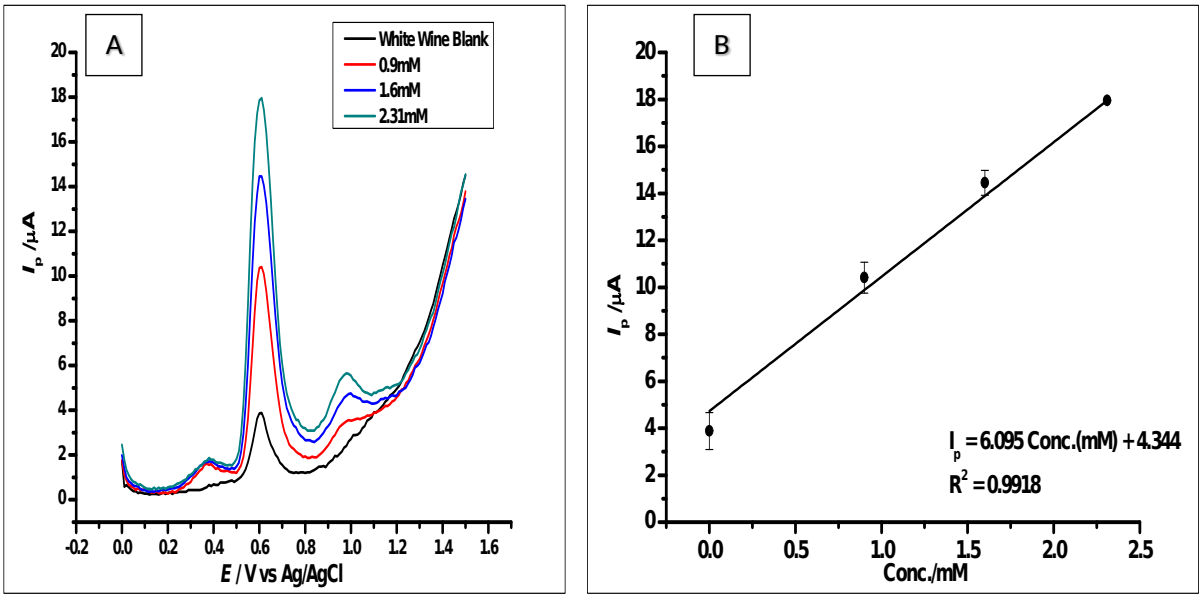

Fig. 12. (a) Voltammograms of aliquots of 1 x 10^{-2} mol L^{-1} of GA added into White Wine using a standard addition method **(b)** Calibration curve of the standard addition of Gallic acid.

S13. Voltammograms of GA determination in Wine Samples

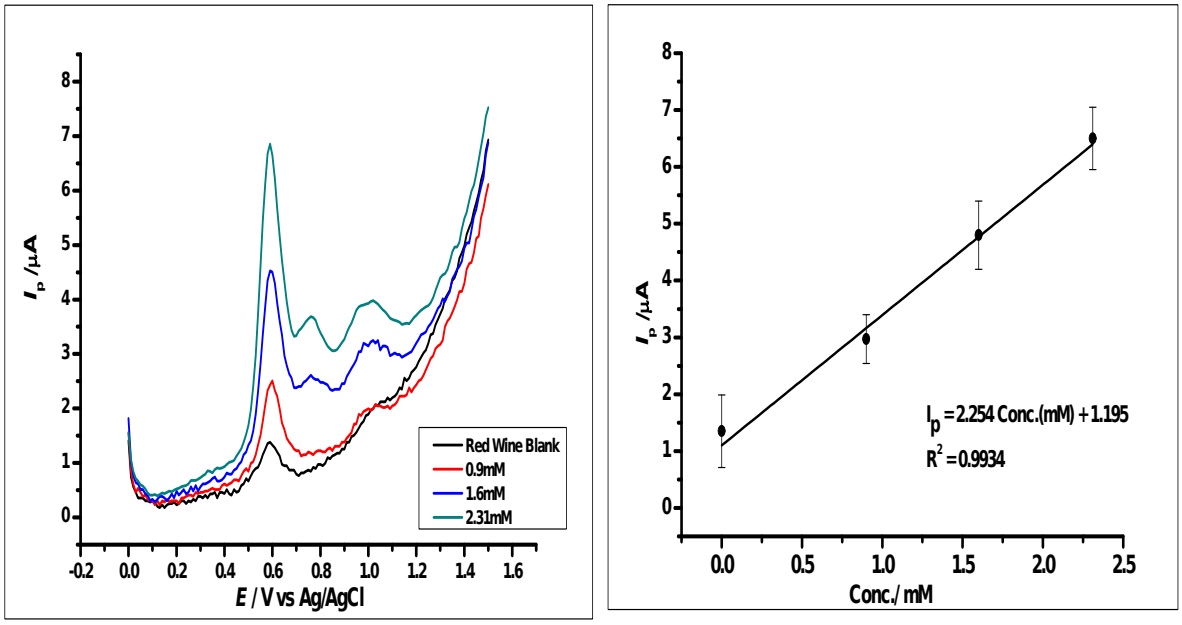

Fig 13. (a) Voltammograms of aliquots of 1 x 10^{-2} mol L^{-1} of GA added into Red Wine using a standard addition method and the presence of the third peak.

S14. HPLC Analysis of wine samples to validate the presence of GA in the Wines.

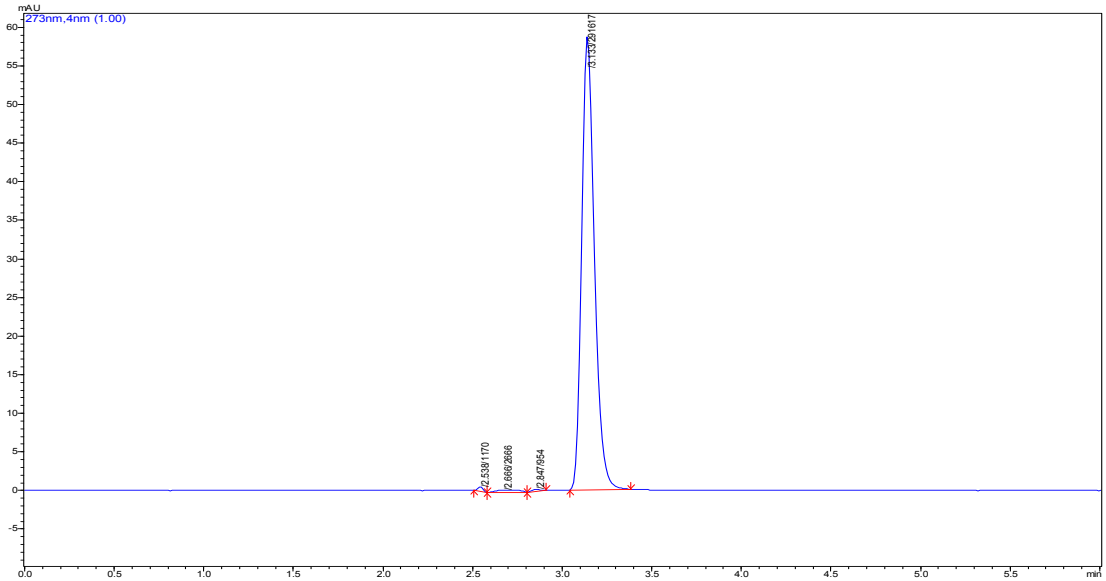

Fig 14. (a) Chromatogram of Gallic acid standard at retention time 3.13 mins. Giving the time Gallic acid would be expected in a Red or White wine.

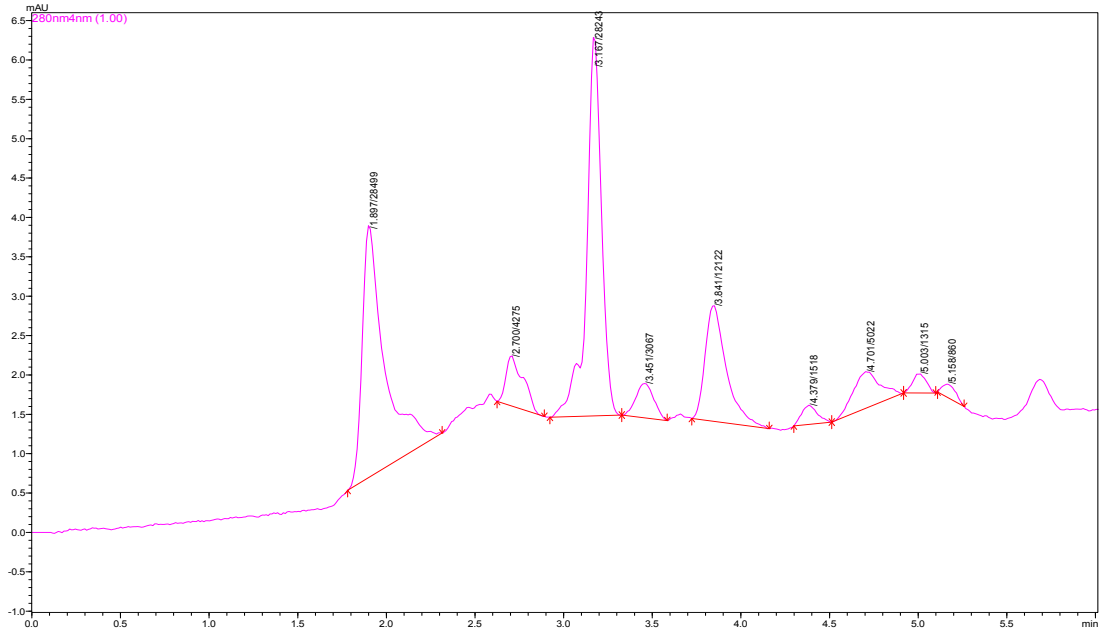

Fig 14. (b) Chromatogram of Red Wine showing the Gallic acid peak at retention 3.16 min.

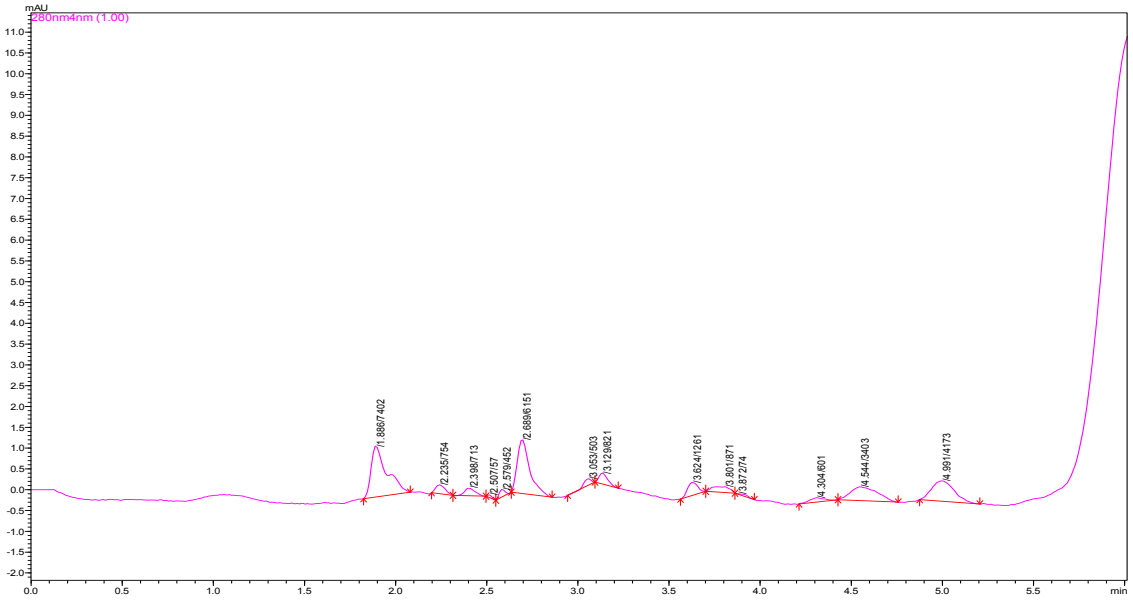

Fig 14. (c) Chromatogram of White Wine showing the Gallic acid peak at the retention time 3.12 min